THE EFFECTS OF WATER CONTENT OF ARTICULAR CARTILAGE ON BIOMECHANICAL PROPERTIES AND MRI IMAGE

TAN KAE CHIN

UNIVERSITI TEKNIKAL MALAYSIA MELAKA

UNIVERSITI TEKNIKAL MALAYSIA MELAKA

© Universiti Teknikal Malaysia Melaka

THE EFFECTS OF WATER CONTENT OF ARTICULAR CARTILAGE ON BIOMECHANICAL PROPERTIES AND MRI IMAGE

TAN KAE CHIN

A report submitted
in fulfillment of the requirement for the degree of
Bachelor of Mechanical Engineering

UNIVERSITI TEKNIKAL MALAYSIA MELAKA

Faculty of Mechanical Engineering

UNIVERSITI TEKNIKAL MALAYSIA MELAKA

2019

© Universiti Teknikal Malaysia Melaka

DECLARATION

I declare that this project report entitled “The effects of water content of articular cartilage on biomechanical properties and MRI image” is the result of my own work except as cited in the references

Signature : .....

Name : .....

Date : .....

UTeM
اونيۏرسيتي تيکنيکل مليسيا ملاک
UNIVERSITI TEKNIKAL MALAYSIA MELAKA

© Universiti Teknikal Malaysia Melaka

APPROVAL

I hereby declare that I have read this project report and in my opinion this report is sufficient in terms of scope and quality for the award of the degree of Bachelor of Mechanical Engineering.

Signature :. .....

Name of Supervisor : .....

Date : .....

UNIVERSITI TEKNIKAL MALAYSIA MELAKA

© Universiti Teknikal Malaysia Melaka

DEDICATION

With my deepest gratitude that I dedicate this thesis to my beloved parents and family for their endless love and support. This is also dedicated to my respectful supervisor for his mentorship throughout this study, examiners, lecturers and all my friends for their unwavering support over the years.

UNIVERSITI TEKNIKAL MALAYSIA MELAKA

© Universiti Teknikal Malaysia Melaka

ABSTRACT

Osteoarthritis (OA) is a major health issues among the population. It causes pain in human joint when moving. The main cause of OA is degeneration of articular cartilage. The earliest stage of OA resulted in the alteration of the biomechanical properties of cartilage elastic modulus and permeability. Hence, the ability to detect the disease at its earlier stage is crucial for early detection of the disease. MRI technique is common used to evaluate the articular cartilage and reflects its biomechanical and histological complexity. However, most of the diagnoses were performed at the progressive stage of OA. Besides that, high field MRI was used in most of the previous works and current clinical procedures. High field MRI required significant purchase and high maintenance cost. Therefore, this study aimed to investigate the potential application of low field MRI image in order to examine the condition of articular cartilage. Cartilage specimens obtained from the bovine femoral head were scanned using 0.18 T MRI. Gradient echo sequence of the low field MRI was found as the most suitable sequence to image the cartilage. The images of cartilage were characterized based on the intensity of the greyscale. Creep indentation test was then conducted on the cartilage specimens and follow by the indentation test was simulated using finite element method. The biomechanical properties of cartilage elastic modulus and permeability were characterized by integrating the experimental indentation test data and computational finite element model. The average elastic modulus was found to be 0.39 ± 0.14 MPa while the permeability was $22.59 \pm 14.85\text{x}\,10^{-15}$ m^4/Ns. Correlation analyses were performed to examine the relationship between greyscale of MRI image and biomechanical properties of elastic modulus and permeability of the cartilage. It was found that the cartilage greyscale was moderately correlated with cartilage biphasic elastic modulus (r= 0.617) and lower correlation was observed with the permeability (r= 0.593). Thus, present results indicate that the low field MRI have the potential and provide promising insight to determine the condition of articular cartilage. It could be further develop to serve as an early detection of OA disease.

© Universiti Teknikal Malaysia Melaka

ABSTRAK

Osteoartritis ialah salah satu isu kesihatan yang menyebabkan kesakitan pada sendi manusia. Punca utama osteoartritis merupakan degenrasi tulang rawan artikular. Pada peringkat awal osteoartritis, ciri-ciri biomekanikal elastik and kebolehtelapan tulang rawan akan mengalami perubahan. Kajian mendalam mengenai tulang rawan telah banyak dijalankan semasa perubahan patologi pada tisu rawan. Oleh itu, keupayaan untuk mengesan osteoartritis pada peringkat awal adalah penting untuk intervensi awal bagi rawatan penyakit ini. Kaedah pengimbas pengimejan resonans magnetik digunakan secara meluas untuk mengkaji keadaan tulang rawan artikular. Walau bagaimanpun, diagnosis ini biasa dijalankan pada peringkat perkembangan osteoartritis. Kebanyakan kajian lanjutan terdahulu dan prosedur klinikal semasa telah dijalankan dengan mengaplikasikan medan pengimejan resonans magnetik berkekuatan tinggi yang memerlukan kos pembelian dan penyelenggaraan yang tinggi. Oleh itu, kajian ini bertujuan untuk mengkaji potensi pengimejan resonans magnetik berkekuatan rendah dalam pemeriksaan keadaan tulang rawan. Tulang rawan daripada humerus sendi bahu lembu telah digunakan untuk pengimejan dengan mengaplikasikan medan pengimejan resonans magnetik yang berkekuatan serendah 0.18 T. Di dalam kajian ini, didapati urutan gema kecerunan adalah urutan yang paling sesuai dalam pengimejan resonans magnetik berkekuatan rendah untuk mengkaji tulang rawan. Imej tulang rawan ini kemudian dicirikan mengikut keamatan skala kelabu. Ujian lekukan dijalankan untuk mendapatkan data daripada eksperimen dan model unsur tak terhingga telah dibangunkan daripada pengukuran geometri tulang rawan. Kajian mengkaji ciri-ciri biomekanikal tulang rawan dilakukan dengan mengintegrasi data eksperimen ujian lekukan dan pengkomputeran unsur tak terhingga. Nilai purata elastik modulus tulang rawan adalah 0.39 $\pm$ 0.14 MPa manakala purata untuk kebolehterapan adalah 22.59 $\pm$ 14.85 x 10^{-15} m^4/Ns. Analisis korelasi telah dikaji untuk mengenalpasti hubungan antara skala kelabu dan sifat biomekanikal modulus elastik dan kebolehtelapan tulang rawan. Berdasarkan hasil kajian, skala kelabu tulang rawan menunjukkan hubungan sederhana dengan modulus elastik (r=0.617) dan hubungan yang lebih rendah diperhatikan pada kebolehtelapan (r=0.593). Hasil dari kajian ini menunjukkan pengimejan resonans magnetik yang berkekuatan rendah berpontensi untuk menentukan keadaan tulang rawan artikular. Pendekatan ini boleh dikaji secara mendalam bagi memberi panduan kepada intervensi rawatan yang awal dalam bidang penyelidikan penyakit osteoartritis.

© Universiti Teknikal Malaysia Melaka

ACKNOWLEDGEMENT

I would like to express my deepest appreciation to my supervisor Prof Madya Dr Mohd Juzaila Bin Abd Latif for giving me this opportunity to do final year project with him. He never hesitated to give me advice and guidance whenever I confronted problems. I am thankful for his patience and advice while leading me in this project.

I would like to thank my course mates for giving me their support, patience and encouragement. Finally, I would like to thank my family for their support.

UNIVERSITI TEKNIKAL MALAYSIA MELAKA

© Universiti Teknikal Malaysia Melaka

TABLE OF CONTENTS

© Universiti Teknikal Malaysia Melaka

© Universiti Teknikal Malaysia Melaka

UNIVERSITI TEKNIKAL MALAYSIA MELAKA

© Universiti Teknikal Malaysia Melaka

LIST OF TABLES

UNIVERSITI TEKNIKAL MALAYSIA MELAKA

© Universiti Teknikal Malaysia Melaka

LIST OF FIGURES

UNIVERSITI TEKNIKAL MALAYSIA MELAKA

© Universiti Teknikal Malaysia Melaka

UNIVERSITI TEKNIKAL MALAYSIA MELAKA

© Universiti Teknikal Malaysia Melaka

LIST OF ABBEREVATIONS

CAX4RP	Four-node bilinear displacement and pore pressure element, reduce integration
DICOM	Digital imaging and communications in medicine
ECM	Extracellular matrix
FE	Finite element
GRE	Gradient echo
MRI	Magnetic resonance imaging
OA	Osteoarthritis
PBS	Phosphate buffer saline
SE	Spin echo

UNIVERSITI TEKNIKAL MALAYSIA MELAKA

© Universiti Teknikal Malaysia Melaka

LIST OF SYMBOL

k	=	Permeability
E	=	Modulus of elasticity
v	=	Poisson's ratio
e	=	Void ratio
T	=	Tesla
°C	=	Celsius

UNIVERSITI TEKNIKAL MALAYSIA MELAKA

© Universiti Teknikal Malaysia Melaka

CHAPTER 1

INTRODUCTION

1.1 BACKGROUND

Osteoarthritis (OA) is a human joint disease worldwide. OA commonly happens in the part of body that has weight-bearing joints, for example, hips, knees and spine (Taruc-Uy and Lynch, 2013). Fingers, neck, wrist and large toe also affected. The OA patient will feel joint aching while moving and pain after overuse. In United States, more than 40 million of population affected by OA and bring disability nationwide (Hansen et al., 2012). Approximately 10% of the persons over 65 years old or 2% of the adult population are suffer with the OA (Felson et al., 2016).

UNIVERSITI TEKNIKAL MALAYSIA MELAKA

There are several factors cause the OA such as ageing, previous joint injury and obesity. Ageing plays a fundamental role in the idiopathic OA. Therefore, OA is the highly prevalent chronic disease among the senior citizen (Liess et al., 2002). While moving, the patient will feel pain and feel relieve by rest. Because of this, the movement of the patient is restricted and reduce in functional capacity. After some time, the joint will worn and the pain will more significant. In fact, the main cause of OA is degeneration of articular cartilage. Figure 1.1 shown the normal knee joint and OA knee joint.

© Universiti Teknikal Malaysia Melaka

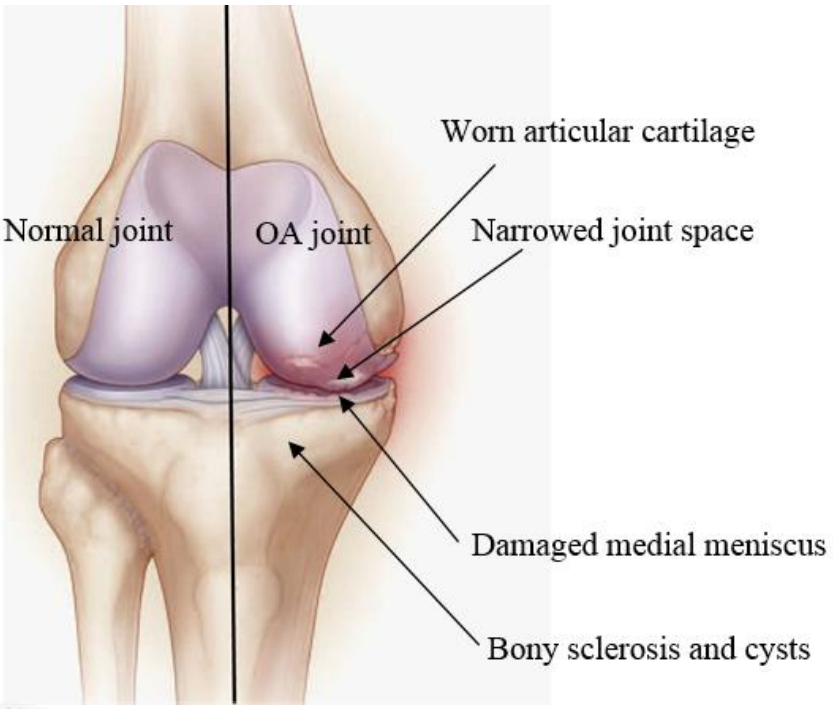

Figure 1.1: Normal knee joint and osteoarthritis knee joint (Uth and Trifonov, 2014).

Articular cartilage is the layer that covered the extremity bone in joint. It is a biphasic medium consists of fluid phase and solid phase. Water is the main component in the fluid phase and it fills the gap between solid matrix. It contributes about four fifths of the wet weight of the articular cartilage (Armstrong and Mow, 1982). The mechanical properties of articular cartilage strongly correlated with the water content of the tissue. An elevated water content in the cartilage tissue characterized the early form of OA. Water content in the cartilage decrease with ageing. This causes the permeability, *k* will decreased and the Modulus of elasticity, *E* will increased (Armstrong and Mow, 1982).

Magnetic resonance imaging (MRI) is a non-invasive imaging method to diagnose OA and visualize articular cartilage (Eckstein et al., 2006). The magnetic field strength of MRI can be categorised into low field MRI (<1.5 T), high field MRI (1.5 T- 7.0T) and ultra-high field MRI (>7 T). From the previous study, the results shown similar diagnostic

© Universiti Teknikal Malaysia Melaka

accuracy, specificity and sensitivity when do the comparison between the high field MRI machine, low field and intermediate while imaging the extremity (Roemer et al., 2010).

1.2 PROBLEM STATEMENT

In the early stage of osteoarthritis, decreasing of the thickness of the articular cartilage is not significant but the decreasing of the biomechanical properties are significant. Proteolytic breakdown of the cartilage matrix, the fibrillation and erosion of the cartilage surface, and the beginning of the synovial inflammation are the three broad stages of progression of OA. The articular cartilages have limited regenerative capability. Therefore, early detection of OA could provide better early prevention of OA. This can reduce the disability and pain of the patient.

In the previous studies, the mechanical compressive parameters of the articular cartilage decreases between 20% to 80% in the early OA stage (Nieminen et al., 2004, Kumar et al., 2018). The early changes of the articular cartilage might undetectable using common clinical methods because the cartilage loss and marginal superficial changes are not significant. The evaluation of the interstitial water content of articular cartilage were carried out. T_1 relaxation time of MRI is strongly correlate to the water content of articular cartilage (Berberat et al., 2009). This method can examine degeneration of cartilage by approximating the changes in actual water content.

However, the low field MRI is not popular being use in examination of cartilage. In addition, most of the studies were investigated using the fresh and healthy cartilage where the water content was in the range of 70% to 80% (Berberat et al., 2009, Shiguetomi-Medina et al., 2017). The effects of water content on biomechanical behaviour of articular

© Universiti Teknikal Malaysia Melaka

cartilage are yet to be explored. Therefore, this study aims to examine the effects of water content on characterised biomechanical properties and MRI image of articular cartilage.

1.3 OBJECTIVE

1. To examine the effect of water content on biomechanical properties of articular cartilage.
2. To examine the effect of water content on MRI image of articular cartilage.

1.4 SCOPE OF PROJECT

1. The cartilage specimen used in this study was obtained from bovine femoral head.
2. Characterization of modulus of elasticity, E and permeability, k of the cartilage were carried out using a combination of indentation test and finite element analysis (FEA).
3. The cartilage specimen was scanned using low field 0.18 T MRI system.
4. Characterization the greyscale of MRI image of articular cartilage was performed using MATLAB software.

UNIVERSITI TEKNIKAL MALAYSIA MELAKA

© Universiti Teknikal Malaysia Melaka

1.5 GENERAL METHODOLOGY

In order to achieve the objective, there are procedures need to be carried out. Before starting the experiment, the literature review related to the study were reviewed. The journals, articles or any materials related to the research were reviewed.

The specimen and materials needed were prepared. The specimen used in this research was articular cartilage of bovine femoral head. The bovine hip joint bought from the local abattoir in Jasin. The flesh was removed by using scalpel. Then, the joint was cut out by using electric handsaw. The excess tissues and damaged surfaces were removed. After that, the joint was cut into slices and drilled out the small piece of bone that attached the cartilage by using electric hand drill. The bone was removed by using scalpel. The specimens were put in the room to dehydrate and get the different water content. During preparation process, the specimen need to soak in the phosphate buffered saline (PBS) to prevent dehydration. PBS is a solution that contains sodium chloride, sodium phosphate, potassium chloride and potassium phosphate. It was prepared by dissolved the PBS tablet in the distilled water with the ratio of 1 tablet in 100 ml of distilled water.

UNIVERSITI TEKNIKAL MALAYSIA MELAKA

The specimens with different water content were scanned with the 0.18 T low field MRI Esaote C-scan MRI machine. The images generated from the MRI are processed using Matlab software. Based on the image grayscale, the details of the cartilage were characterize. After that, the cartilage specimens were used to do the indentation test. The indentation test is to study the time dependent and the deformation of the articular cartilage. Then, the model of articular cartilage was analysed by using ABAQUS software. The biomechanical properties, permeability, k and modulus of elasticity, E were characterized from the result. Finally, the correlation between the grayscale, permeability, k and modulus of elasticity, E were plotted in the graph.

© Universiti Teknikal Malaysia Melaka

The experimental and computational result were compared and discussed. A report for this research was written at the end of the research. The methodology of this research was summarized in the flow chart as shown in Figure 1.2.

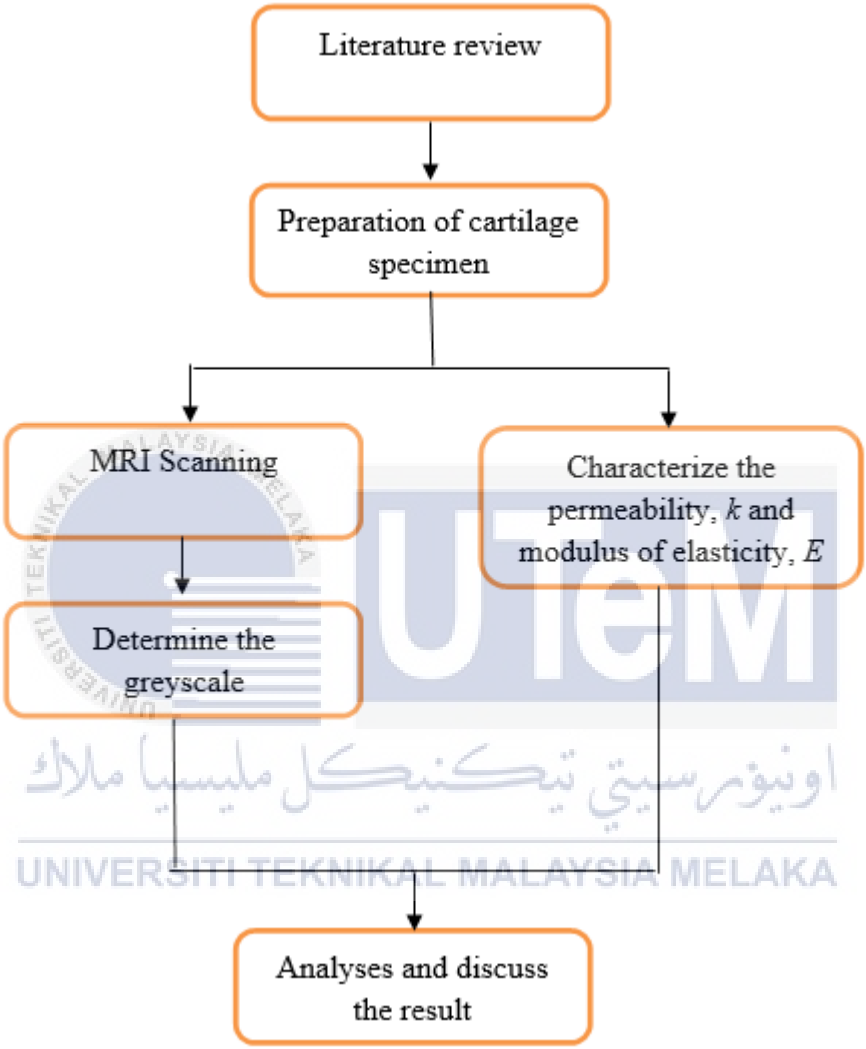

Figure 1.2 Flow chart of the general methodology.

© Universiti Teknikal Malaysia Melaka

CHAPTER 2

LITERATURE REVIEW

2.1 Synovial Joint

Synovial joint plays an important role in musculoskeletal system. The synovial joints characterized by articular cartilage and bathed in synovial fluid (Raleigh et al., 2017). It provides the body stability, movement and manipulate objects within the immediate environment (Eckstein et al., 2006). The key function of the synovial joint is to ease the implementation of the basic mechanical task of motion (Mow and Lai, 1980). Synovial joint consents the movement between the long bones. Knees, hips, shoulders, elbows, and phalangeal are the parts consist of synovial joints.

UNIVERSITI TEKNIKAL MALAYSIA MELAKA

2.1.1 Types of Synovial Joint

Human synovial joints can be categorized into six types which are condyloid joint, ball and socket joint, pivot joint, hinge joint, plane joint and saddle joint. Figure 2.1 shown the types of synovial joint in human body.

© Universiti Teknikal Malaysia Melaka

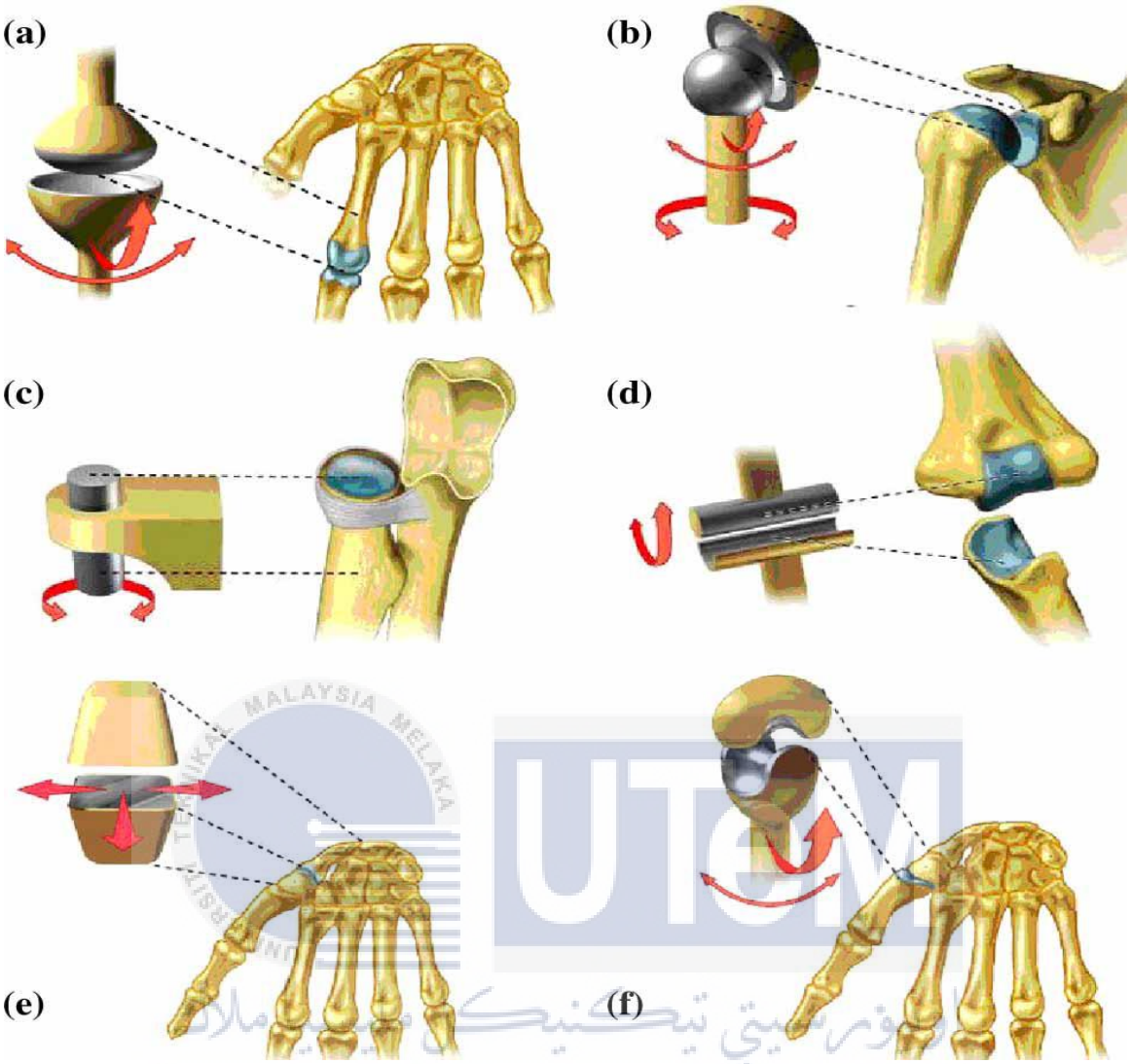

UNIVERSITI TEKNIKAL MALAYSIA MELAKA

Figure 2.1: Types of synovial joints. (a) condyloid joint (b) ball-and-socket joint (c) pivot joint (d) hinge joint (e) planar joint (f) saddle joint (Yang et al., 2008).

Pivot joint is the joint that allow rotational movement. It consists of a rounded end bone that can fit into a ring formed by the other bone. Joint of neck vertebrae and wrist are the example of the pivot joint which allow the head to turn left and right and palm turn up and down. Hinge joints like the hinge of door. It enables swinging motion and bending motion. Hinge joints usually found at knees, elbows, ankles, toes and fingers. For saddle

© Universiti Teknikal Malaysia Melaka

joint, both end of the articulating bones have the same saddle shape which concave and convex portions that fit together. One of the example of the saddle joint is thumb, it allows motion in forth, back, up and down. Plane joint also known as gliding joint usually found in the carpal bones in the hand and the tarsal bones of the foot. It allows the movement more flexible because it can move in many directions. Condyloid joint also known as ellipsoid joint. Knuckle joints of the hand and radiocarpal joint of the wrist are the examples of the condyloid joint. It allows angular movement along two axes. First movement is bending and strengthening while the second movement is side to side movement, which allow to spread apart and bring. This can be clearly seen at the fingers. Ball and socket joint classified as multiaxial joint as it possible to move in all directions. It usually found at the shoulder joint and hip joint.

2.1.2 Anatomy of Synovial Joint

There are three fundamental parts in synovial joint that are articular cartilage, synovial membrane and joint cavity. The interval between the bones is known as joint cavity. It filled with a viscous fluid known as synovial fluid that supplies nourishment to the articular cartilage and as a lubricant at the joint (Huber et al., 2000). Synovial membrane is a layer of connective tissue that lines the cavities of joint, tendon sheaths, and bursae. Articular cartilage is a layer of specialized connective tissue with unique characteristics (Carballo et al., 2017). Anatomy of synovial joint is shown in Figure 2.2.

© Universiti Teknikal Malaysia Melaka

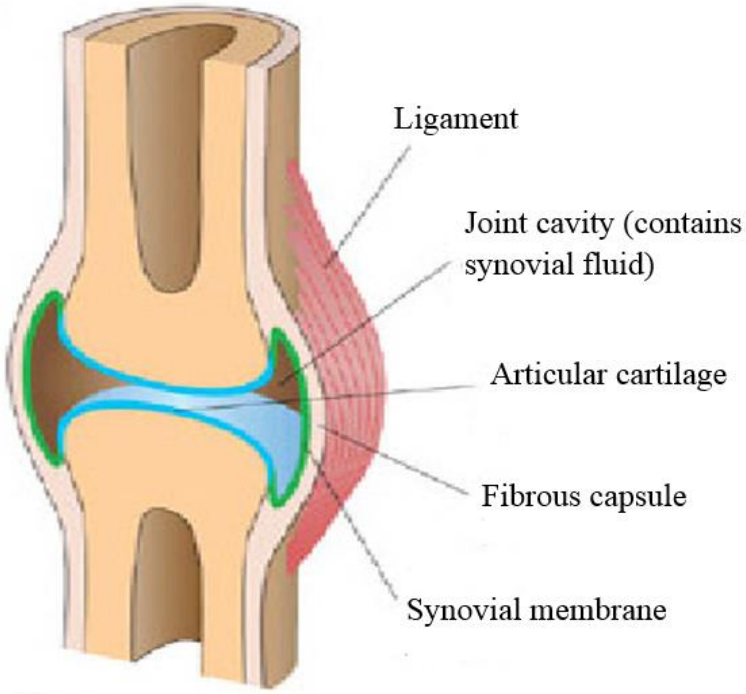

Figure 2.2: Anatomy of synovial joint (Sotres and Arnebrant 2013).

The function of the synovial joint is provide the ability to the body to move and maintain posture (Eckstein et al., 2006). The function of the articular cartilage is to lubricate the bones when moving. It allows the articulating joint moves smoothly and without damage the underlying bone tissues. Synovial membrane secretes synovial fluid to lubricate the joint.

UNIVERSITI TEKNIKAL MALAYSIA MELAKA

© Universiti Teknikal Malaysia Melaka

2.2 Osteoarthritis

Osteoarthritis (OA) is a joint disease among the senior citizen and causes disability. OA usually affected weight bearing joints. It caused by degeneration and eventual loss of articular cartilage tissue (Liess et al., 2002). According to the WHO Scientific Group on Rheumatic disease, about 10% of the world's population who are 60 years old and above are suffered OA (Pereira et al., 2011). OA is characterized by cartilage loss, subchondral bone changes, low grade synovitis and other joint tissue alterations (Zamli and Sharif, 2011). The symptoms of OA can vary from mild to severe joint pain which can involve single or multiple joints. Symptom will be more significant by movement or extensive use.

Early stage of OA is hard to detect because the cartilage lacks of nerves. The cartilage can be damaged without any directly associate pain (Eckstein et al., 2006). Cartilage in the joint act as the shock absorber and reduces the friction between the bones due to its rubbery characteristic. OA causes the cartilage loss the stiffness and elasticity. It causes the cartilage ease to damage. After some times, the cartilage will tear and worn. New bony or spurs will grow due to the damaged of cartilage (Taruc-Uy and Lynch, 2013). Inflammatory process may occurs because some of the bone or cartilage chip off and float around in the joint. This will develop the further damage of the cartilage. Figure 2.3 shown the schematic view of healthy joint and osteoarthritis joint.

UNIVERSITI TEKNIKAL MALAYSIA MELAKA

© Universiti Teknikal Malaysia Melaka

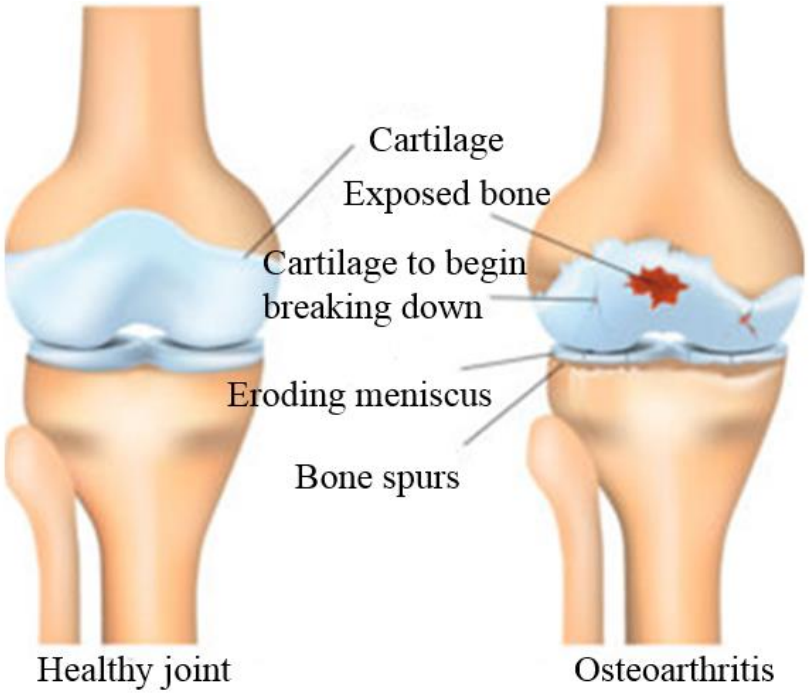

Figure 2.3: Schematic view of healthy joint and osteoarthritis joint (https://drjeffpadaleckimd.com/).

UNIVERSITI TEKNIKAL MALAYSIA MELAKA

2.2.1 Causes

The development of OA is combine of biochemical, cellular and mechanical processes (Taruc-Uy and Lynch, 2013). There are various causes of OA including cartilage degeneration, ligament derangements, increased mechanical stress, subchondral bone changes and muscle impairments (Egloff et al, 2012). However, it is well recognized that the main cause of OA is cartilage degeneration. Weight, genetic factors, gender, traumas, age, physical activity, lifestyle and occupational factors increase the risk of OA.

From the previous study, the person who obesity has the higher risk of having osteoarthritis (Felson et al., 1996). For every two units of Body Mass Index (BMI) of weight gain, the risk for knee OA increased by 36% (Lementowski, 2014). Joint loading

© Universiti Teknikal Malaysia Melaka

increasing as the weight increasing. Therefore, obesity will cause the deleterious effect on the joint (Kulkarni et al., 2016). Excess load acting on the joint will breakdown the cartilage. The women that 50 years old and above have a higher prevalence of OA than men (Srikanth et al., 2005). One of the factor is hormonal different between men and women. Estrogen is a type of hormone that brings benefits to the cartilage. For postmenopausal women, the estrogen decreases at that time. Therefore, this increases the risk of OA (Hame and Alexander, 2013).

2.2.2 Diagnosis

Osteoarthritis can be avoid or lessen long term disability by early diagnosis. Joint pain is the common sign of OA. When moving, the pain tends to worsen. Diagnosis of OA can be conducted through medical history and physical examination according to the symptoms of pain, joint swelling and reduction in the movement.

UNIVERSITI TEKNIKAL MALAYSIA MELAKA

The most common diagnosis methods are imaging test and laboratory test. Imaging test includes X-ray, magnetic resonance image (MRI), ultrasound, and arthroscopy (Felson et al., 1996). Through the imaging test, the space between the bones can be clearly seen. Simple radiography can evaluate the cartilage and determine the degenerative disease (Rodrigues and Camanho, 2010). By using magnetic resonance imaging (MRI) to examine the cartilage, the early stage of OA can be indicate. Laboratory test is undergoes the joint fluid analysis. The fluid will be draw out from the affected joint and determine whether it is inflammation or not.

© Universiti Teknikal Malaysia Melaka

2.2.3 Treatment

There is no cure for osteoarthritis, but treatment helps to relieve the symptom and does not get worse. The treatment for OA including physical therapy, pharmacologic and surgical (Taruc-Uy and Lynch, 2013). The treatment options depend on the health need which include medical history, level of pain and the influence of OA in daily life.

Joint preserving surgery and total joint replacement are the common surgery for osteoarthritis treatment (Egloff et al., 2012). Joint preserving surgery is to preserve the deteriorating joint in order to delay or avoid joint replacement surgery. This can relieve pain and improve function. Total joint replacement is replace the damaged joint with an artificial joint called prosthesis.

Physical therapy has significantly improve the functional ability, self -perceptions of pain and stiffness for patients with OA (Deyle et al., 2000). Assistive devices such as walking cranes, braces and footwear interventions may improve the patient's ability to carry out daily routine. Gait modifications, muscle strengthening and weight loss also help to reduce the symptom of OA (Egloff et al., 2012).

UNIVERSITI TEKNIKAL MALAYSIA MELAKA

Medication can control the symptoms of OA. The painkillers are to relieve and control the pain. Topical capsaicin cream consists of chili pepper. It produces warmth when applied on the joint. Capsaicin cream works by blocking the nerves that send pain messages in the treated area. Non-steroidal anti-inflammatory drugs (NSAIDs) are the mainstay for the treatment for the OA. It works as a painkiller and reduces the inflammation.

© Universiti Teknikal Malaysia Melaka

2.3 Articular Cartilage

Articular cartilage is a type of strong and flexible fine connective tissue that covers the extremity of the articulating bone in synovial joint. It does not have blood vessels, nerves or lymphatics (Fox et al., 2012). An healthy articular cartilage is smooth, uniform, glassy appearance and bluish white in colour (Lees and Partington, 2016). It appears bluish white in colour due to no blood supply. It plays an important role in frictionless movement of the surfaces of articulating joint (Huber et al., 2000). Articular cartilage mostly consists of water, proteoglycans and complex mesh of collagenous fibers. All the composition components effect the biomechanical properties of the articular cartilage.

The movements of the body requires a smooth, lubricated and low friction surface at the end of the articulating bones. The resulting compressive and tensile forces able to disperse to the underlying subchondral bone due to its specific material characteristics. Complex lubrication mechanisms are facilitate during articulation to keep the shear stresses low.

UNIVERSITI TEKNIKAL MALAYSIA MELAKA

© Universiti Teknikal Malaysia Melaka

2.3.1 Composition

Articular cartilage is biphasic nature that made up of solid and fluid phases. Fluid phase made up of water and electrolytes. It fills the spaces between the solid matrix. Wet weight of the articular cartilage mainly contribute by the water (Lees and Partington, 2016). The solid phase divides into two main components that are chondrocytes and extracellular matrix (ECM). ECM consists of proteoglycans, collagen fibres and non-collagenous protein.

Water is the main component in the articular cartilage. It contributes up to four fifths of the wet weight of the articular cartilage (Carballo et al., 2017). Its concentration decreases from 80% at superficial zone to 65% in the deep zone (Fox et al., 2012). Mechanical properties of the articular cartilage correlated with the interaction of water with the matrix macromolecules (Buckwalter et al., 2005). Transportation and distribution of nutrient to chondrocytes depend on the flow of water. It also provides lubrication in the joint. The hydraulic pressure of water plays a significant role in the load support of articular cartilage.

UNIVERSITI TEKNIKAL MALAYSIA MELAKA

Proteoglycan is the second largest group of macromolecules in the ECM. It contributes up to 15% of the wet weight of articular cartilage. It consists of a protein core and one or more glycosaminoglycan. Glycosaminoglycan is the long unbranched polysaccharide chain that contain an amino sugar in repeating disaccharides form. It consists of hyaluronic acid, chondroitin sulfate, keratin sulfate and dermatan sulfate. Proteoglycans have ability to resist compressive load and generate the swelling pressure (Pearle et al., 2005). Figure 2.4 shown the diagram of the proteoglycan aggregate and aggrecan molecule.

© Universiti Teknikal Malaysia Melaka

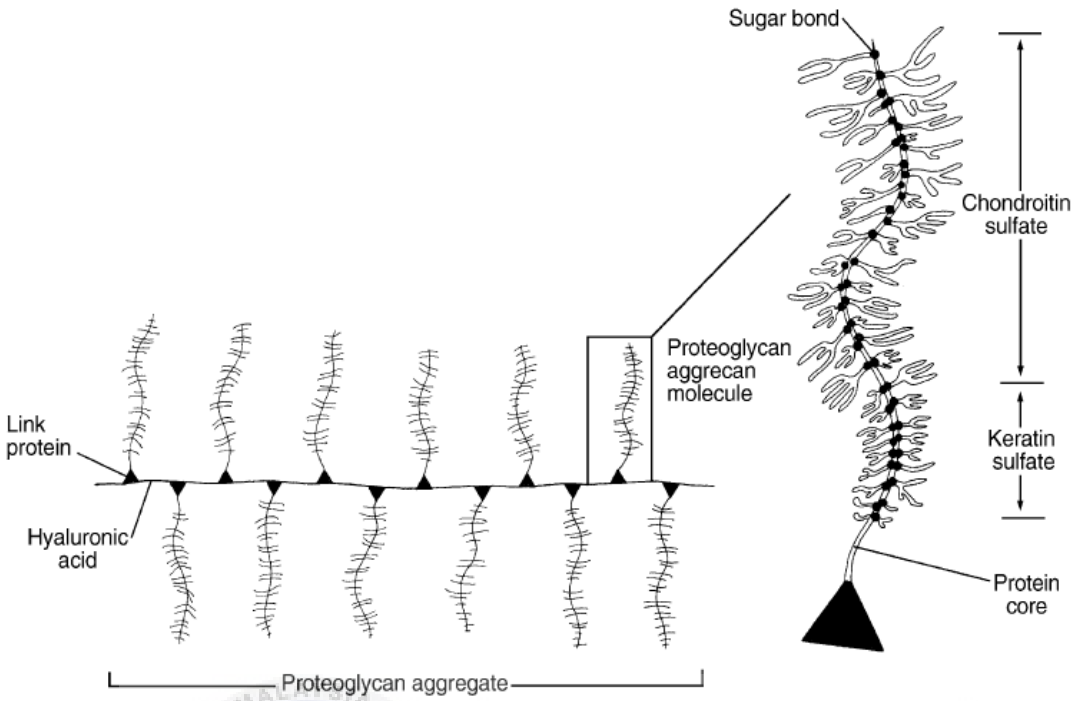

Figure 2.4 Diagram of the proteoglycan aggregate and aggrecan molecules (Pearle et al., 2005).

Collagen accounts for 65% of the dry weight of the articular cartilage (Eyre, 2002). There are 90-95% of the collagen is collagen type II while the rest are types VI, IX, X and XI (Lees and Partington, 2016). Collagen stronger in tension compared to compression due to its slenderness ratio. By using light microscopy, the different collagen orientation in four zones of articular cartilage that are superficial or tangential, middle or transitional, deep or radial and calcified can be visualised. The deeper the zone, the greater the diameter of fibrils diameter and more random the orientation of fibril. The collagen fibrils are arranged parallel to the surface in superficial zone. The collagen fibrils orientation is less organized in middle zone and perpendicular to the surface of the joint in deep zone. Figure 2.5 shown the collagen arrangement in articular cartilage.

© Universiti Teknikal Malaysia Melaka

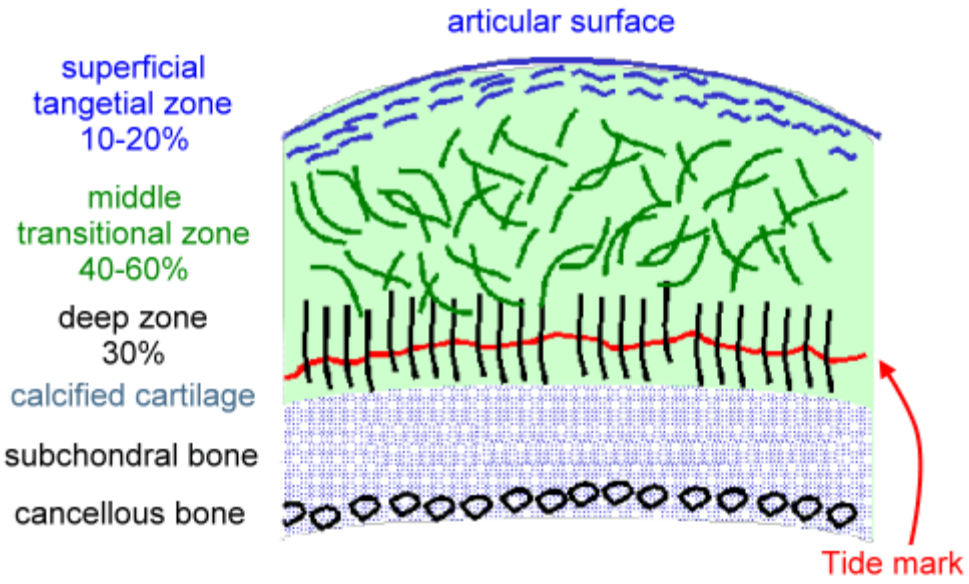

Figure 2.5 Collagen arrangement of the articular cartilage (https://boneandspine.com/).

Chondrocytes play an exclusive role in the development, maintenance, and repair of the ECM. It accounts about 1% of the total volume of the articular cartilage. It is non uniform and vary in number and shape in different zones of the cartilage. Chondrocytes receive the signals transmitted by ECM and regulating their metabolic activity.

UNIVERSITI TEKNIKAL MALAYSIA MELAKA

© Universiti Teknikal Malaysia Melaka

2.3.2 Structure

The structure of articular cartilage is important for biomechanical properties. Articular cartilage made up of four horizontal layers that are superficial or tangential zone, transitional or middle zone, deep zone and calcified cartilage zones (Huber et al., 2000). Figure 2.6 shown the structure of the articular cartilage from the top layer to bottom layer.

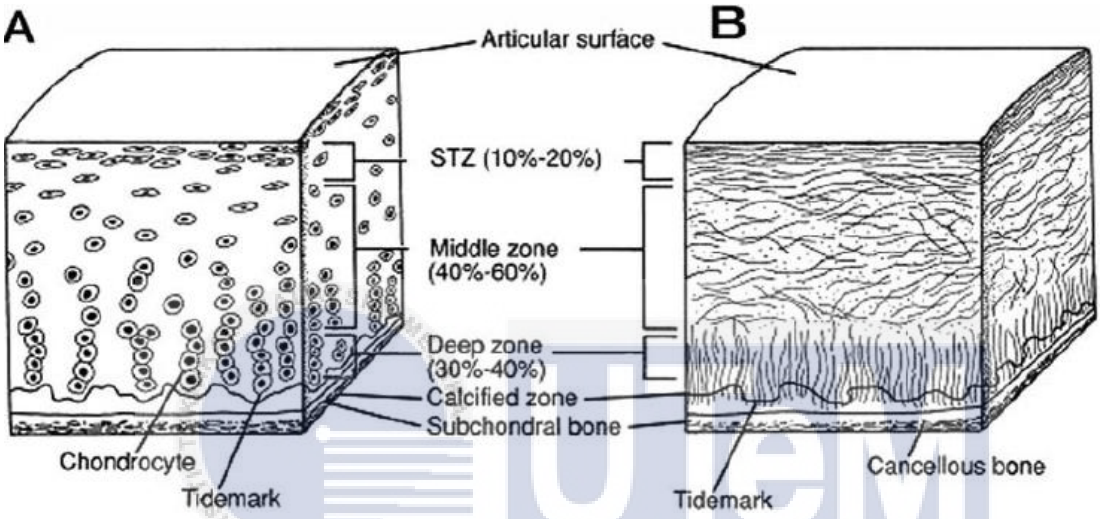

Figure 2.6: Structure of the articular cartilage (Fox et al., 2012).

UNIVERSITI TEKNIKAL MALAYSIA MELAKA

The thinnest zone in the articular cartilage is superficial zone. It provides a smooth gliding surface and protects the deeper layer from shear stresses (Fox et al., 2012). Superficial zone composed of high number of flattened chondrocytes, low number of proteoglycan and high concentration of water. It has the highest collagen content and consists of two layers of collagens. First layer composed of fine fibrils covering the articular surface in the form of thickly packed bundles collagen fibers arranged parallel to each other while second layer contains of collagen fibers arranged perpendicular to the articular surface (Huber et al., 2000).

Transitional zone consists of rounded chondrocytes surrounded by ECM. Collagen fibers in this zone are thicker have random arrangement. The number of proteoglycan in

© Universiti Teknikal Malaysia Melaka

transitional zone is higher than in superficial zone. Chondrocytes in this zone are more rounded than in superficial zone. This zone is the first line of resistance to compressive forces.

The collagen fibrils in the deep zone have the largest diameter and are arranged perpendicular to the articular cartilage. This zone has the highest number of proteoglycan and lowest composition of water. Chondrocytes are typically arranged in columnar orientation, parallel to the collagen fibrils and perpendicular to the joint line. Functionally, the deep zone provides strongest resistance to compressive forces.

Tide mark is an irregular line that separates the deep zone from the calcified zone. It acts as tethering mechanism for the collagen fibrils. Tide mark prevents the collagen fibrils in the non-calcified zone from being sheared of anchorage to the calcified zone. In calcified zone, the collagen fibrils arranged perpendicular to the articular surface. This zone characterized by rounded chondrocytes located in uncalcified lacunae. In addition, it does not have proteoglycan.

UNIVERSITI TEKNIKAL MALAYSIA MELAKA

2.3.3 Properties Characterisation

Characterization of properties of the articular cartilage is important. There are various properties of cartilage including the biomechanical, chemical and biological properties. Therefore, in previous studies, there were many methods to prepare the cartilage specimen and the experimental testing to study the properties of the articular cartilage. However, the biomechanical properties is one of the most important because it plays an important role in attenuation of force in the joint (Lories et al., 2007).

© Universiti Teknikal Malaysia Melaka

2.3.3.1 Specimen Preparation

Preparation of the specimens is critical to avoid the damage of the tissues. Fresh cartilage tissue is fragile and subject to autolysis. It has to handle quickly or keep under moist conditions to retain the properties. To prevent the tissue dry out, the tissue has to cover with saline-moistened gauze or an inverted plastic cup. Phosphate buffer saline (PBS) is used to keep the tissue in fresh and hydrated so as to maintain the actual condition of the cartilage tissues. Furthermore, the blade must be sharp to ease the process.

Different experimental methods have different preservation technique and storage protocol. The specimen stored at 4ºC for less than 48 hours to make sure it is fresh. No freezing was performed to avoid any potential effect of freezing on cartilage matrix (Li et al., 2011).

2.3.3.2 Biomechanical Properties

The common experimental techniques used to evaluate the biomechanical properties of the articular cartilage are indentation test, unconfined compression and confined compression (Park et al., 2004, Hayes and Mockros, 1972). In confined compression, the cartilage sample is placed in an impervious, fluid-filled well and loaded through a porous plate to force the fluid flows vertically. For unconfined compression, the cartilage is loaded using an impermeable plate onto an impermeable chamber and the flow through the cartilage is predominantly radial. For indentation test, an indenter is brought down onto the specimen to evaluate the properties of the specimen (Griffin et al., 2016). However, indentation test is the most often used method to determine the biomechanical properties of the articular cartilage. Figure 2.7 shown the three types of mechanical testing configurations.

© Universiti Teknikal Malaysia Melaka

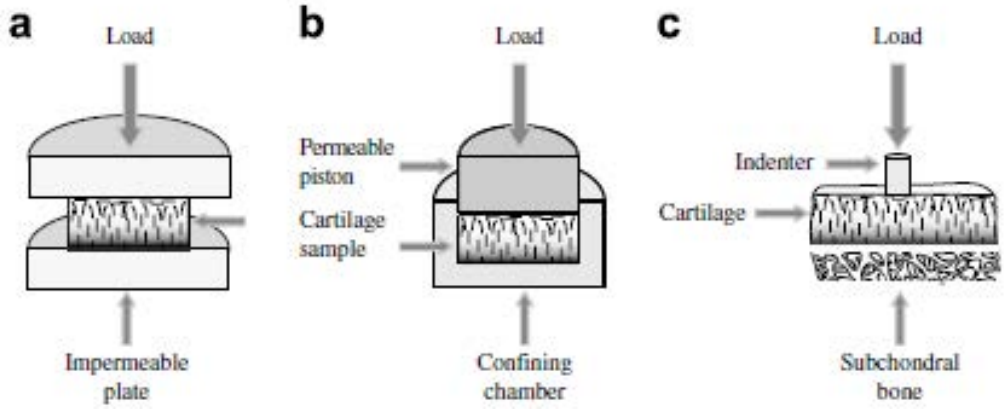

Figure 2.7: Mechanical testing configurations (a) unconfined compression, (b) confined compression and (c) indentation test (Knecht et al., 2006).

Previous study shown that the elastic modulus, *E* decrease with progressive of OA (Peters et al., 2018). From elastic modulus, the biomechanical properties of the articular cartilage can clearly define. It indicates the elastic resistance of articular cartilage to compression and tension. The permeability of articular cartilage contributes many functions such as ability to carry load. It will decreased when the articular cartilage is compressed (Mansour, 1976).

UNIVERSITI TEKNIKAL MALAYSIA MELAKA

The permeability and intrinsic equilibrium elasticity of the articular cartilage are strongly correlation with the water content. As the water content increase, the matrix tissue became softer and more permeable. During deformation, intrinsic mechanical properties of the components controlled the mechanical properties of the articular cartilage (Armstrong and Mow, 1982). The articular cartilage is biphasic, visco-elastic in tension and anisotropic. Its structural complexity and organization related the mechanical properties. These properties are made possible due to up to 70% of the water content is free to move (Lees and Partington, 2016).

© Universiti Teknikal Malaysia Melaka

2.4 Magnetic Resonance Imaging

Magnetic Resonance Imaging (MRI) is the most potential non-invasive means for revealing the structure, composition and pathology of articular cartilage (Nieminen et al., 2004). MRI enables to evaluate the articular cartilage and reflects its biochemical and histological complexity. It can access the articular cartilage tissue that consists of high soft tissue contrast (Rodrigues and Camanho, 2010). Besides that, MRI has the ability to discriminate the articular tissues such as cartilage, menisci and ligaments (Peterfy et al., 2004). The image can obtain in short time and with high resolution (Hayter and Potter, 2011). The black and white contrast image provide the best visualisation and the highest image resolution of articular cartilage (Hardya et al., 2000). Therefore, MRI holds the greatest potential as a tool for joint imaging.

High resolution images of the organs and tissues are created by using magnetic field and radio waves in MRI unit. It uses the magnetic properties in the body to produce image from the part of the body. The magnet in the MRI system produces strong magnetic field that can align the protons in the body. The hydrogen molecules in the tissue resonate because of the radio wave frequency. When the radio frequency is switched off, a signal is emitted and create the MR image.

UNIVERSITI TEKNIKAL MALAYSIA MELAKA

MRI is an important tool to diagnosis the progression of osteoarthritis. It can evaluate the joint structures in axial, coronal and sagittal planes (Raynauld et al., 2004). Degeneration of articular cartilage is the main factor of the progression of OA. Both the morphological changes such as degenerative, severity and rate of loss of the tissue and biochemical changes of the ECM are able to evaluate with the use of MRI (Shapiro et al., 2014).

© Universiti Teknikal Malaysia Melaka

2.4.1 Physical Basic of MRI

A magnetic induction occurs around the wire when the electric current flows through the wire. A strong and constant magnetic field generated by main magnet to which the specimen exposed. The gradient coils are represented by three orthogonal direction (x, y and z). It lies concentric to each other within the main magnet. The gradient coils generated the magnetic field that same direction with the constant magnetic field generated by the magnet. The radio frequency coils act as an antenna in the MRI system. The frequency of electromagnetic energy generated lies within megahertz range. It mounted inside the gradient coils and lied concentric to them and to each other. The radio frequency coil used to transmit the radio frequency energy to the tissue of interest and receive the induced radio frequency signal back from the tissue interest. In addition, the shim coils help to improve the homogeneity within the magnetic field.

Clinical images are generated due to the primary origin of the MR signal comes from hydrogen nuclei. Hydrogen nuclei consists of a single proton that carried a positive charge. The proton constantly spinning so that the positive charge spins around with it. A magnetic field is generating when an electric current is applied. Thus, the protons act like a little bar magnets and have the magnetic field (Currie et al., 2013). When strong external magnetic field is applied, the protons equilibrate into a low energy state and align along the direction of the magnetic field lines. The proton will excite to a higher energy state when the electromagnetic field at the natural or resonant frequency of the proton. The protons relax back to the low energy state when the radio frequency pulse is turn off. The type of proton relaxation and the resultant images is determined by the timing of the radio frequency energy pulses (Macdonald and Peduto, 2000).

UNIVERSITI TEKNIKAL MALAYSIA MELAKA

© Universiti Teknikal Malaysia Melaka

2.4.2 Magnetic Field Strength

The main components of MRI system are magnet, radio frequency (RF) coil, gradient coils, patient seat and a computer system. Magnet is the most important part in MRI system. It functions to produce a large and stable magnetic field strength. Tesla (T) is the unit to rate the strength of the magnet in the MRI system. The magnetic field strength of MRI can be categorised into low field MRI (<1.5 T), high field MRI (1.5 T- 7.0T) and ultra-high field MRI (>7 T).

The characteristics that effected by the magnetic field strength are physical definitions, signal-to-noise ratio (SNR),contrast-to-noise ratio (CNR) and artifacts (Rutt and Lee, 1996). The high field strength has higher signal-to-noise ratio (SNR) and contrast-to-noise ratio (CNR), higher spatial resolution and shorter image acquisition time. These characteristics affect the quality of the MR image.

Most of the studies were conducted using high-field MRI to characterize the structure of joint and biomechanical degradation of articular cartilage (Gudbergsen et al., 2012, Calvo et al., 2001, Luke et al., 2010). High-field MRI allows to demonstrate the early changes of articular cartilage significantly. High-field strength MRI provide a higher SNR and better spatial and spectral resolution. Therefore, the image with better resolution is produced.

High-field MRI has greater potential to detect the structure of the joint compared to the low-field MRI (Przeworski et al., 2016, Woertler et al., 2000). The previous studies shown the high-field MRI produces better quality of image compared to low-field MRI (Taouli et al., 2004, Link et al., 2006). The high-field MRI possible to separate each layers in the joint to examine. However, the higher field strength MRI requires higher cost and

© Universiti Teknikal Malaysia Melaka

safety concerns. Figure 2.8 shown the image of bucket-handle tear of the lateral meniscus in low-field and high-field MR imaging.

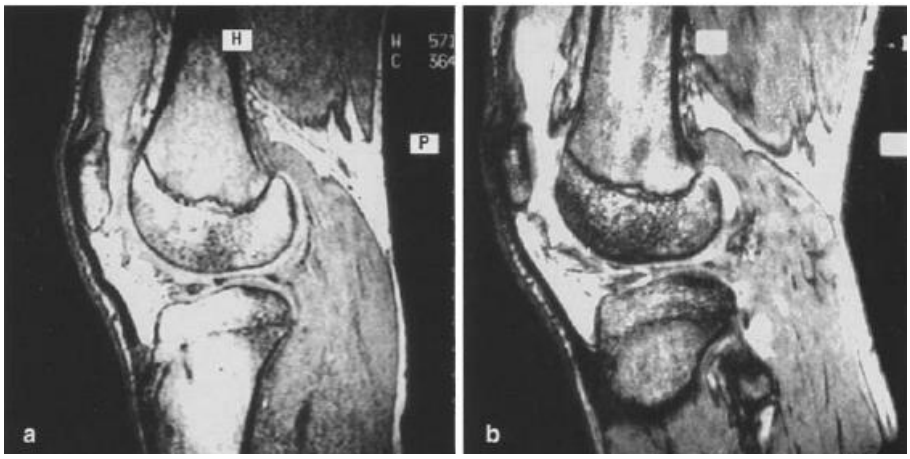

Figure 2.8: MR Image of bucket-handle tear of the lateral meniscus in (a) low-field (0.2 T) and (b) high-field (1.5 T) MR imaging (Kladny et al., 1995).

UTeM
اونيۏرسيتي تيکنيکل ملسيا ملاک
UNIVERSITI TEKNIKAL MALAYSIA MELAKA

2.4.3 MRI Sequence

Pulse sequences are software programs that encode the magnitude and timing of the radiofrequency pulses emitted by the MR scanner, switching of the magnetic field gradient and data acquisition (Ginat et al., 2011). MR sequence is important to assess the cartilage quality. Spin echo (SE) and gradient echo (GRE) are the most common fundamental pulse sequences of MRI. Other MRI sequences are only variation of SE and GRE with different combination of the repetition time, echo time and inversion.

Gradient echo sequence is the simplest type of MRI sequence. It has a series of excitation pulses that separated by a repetition time, TR. After the application of the excitation pulses, data is acquired at some characteristics time. This characteristics time is known as echo time, TE. Spin echo (SE) sequence has an additional 180º refocusing pulse present. This 180 º pulse is exactly halfway between the excitation pulse and the echo.

© Universiti Teknikal Malaysia Melaka

2.4.4 Greyscale Intensity

Greyscale intensity is expressed in the diagnosis of density changes based on brightness and darkness in radiographic image. The dark shade is absence of transmitted or reflected light, while bright shade is the transmission or reflection of light. It is commonly used features in image processing.

Digital Imaging and Communication in Medicine (DICOM) is a format that widely used for the communication and management of medical imaging information. A digital MRI image consists of an array of number, known as greyscale. Each number represents the different shades and contrast resolution. It is expressed as pixel. Figure 2.9 shown the DICOM image with different pixel values.

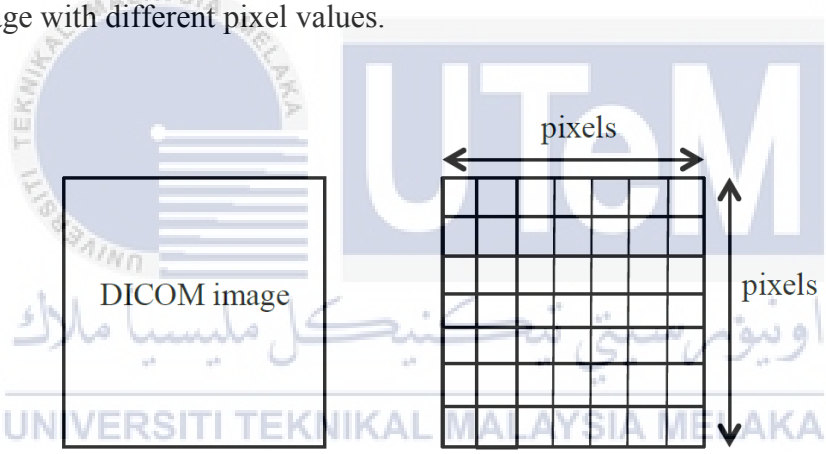

UNIVERSITI TEKNIKAL MALAYSIA MELAKA

Figure 2.9: DICOM image with different pixel values.

The brightness of the pixel is determined by the pixel value in the greyscale image. Byte image is the most common pixel format. 8-bit integer gives a possible values from 0 to 255. Value 0 is black shade and value 255 is the white shade. The values in between form various shades of grey. This similar goes to 2^{12} which can display value up to 4096 and 2^{16} with 65,536.

© Universiti Teknikal Malaysia Melaka

2.5 Low Field MRI Studies of Articular Cartilage

Low field MRI systems assume have a higher cost effective and equivalent reliability compared to conventional high field scanners. The uses of dedicated low field MRI systems increase gradually in orthopaedic applications (Woertler et al., 2000). Low field MRI systems are smaller in size, cheaper, ease of install and allow for diagnoses in short time and in an office setting (Lee et al., 2013). Compared to high field systems, low field or intermediate field MRI recommend as alternative for cost saving reason and more comfortable for patient.

From the previous study, the results shown similar diagnostic accuracy, specificity and sensitivity when do the comparison between the high field MRI machine, low field and intermediate while imaging the extremity (Roemer et al., 2010). There is no great differences in lesion-to-white-matter contrasts between high-field and low-field MRI examination (Wirtz and Aras, 2001). Figure 2.10 shown the MRI image of the infrapatellar and intercondylar at 1.0 T and 1.5 T MRI.

UNIVERSITI TEKNIKAL MALAYSIA MELAKA

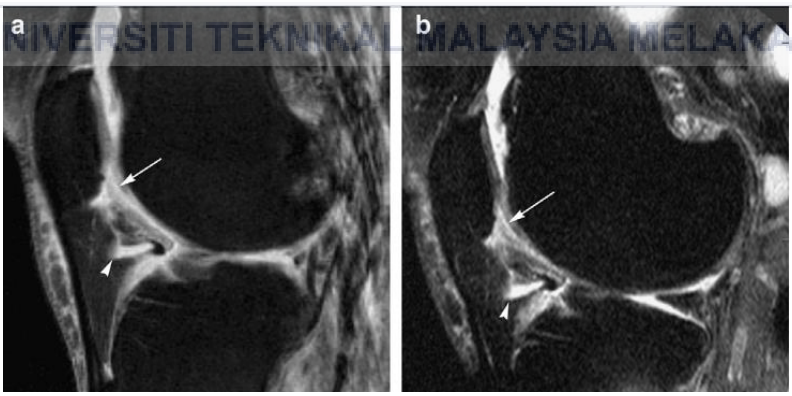

Figure 2.10: Equivalent delineation signal changes in the infrapatellar (a and b, arrow) and intercondylar (a and b, arrowheads) regions (a) Sagittal planes at 1.0 T MRI (b) Same slice on the 1.5 T system (Roemer et al., 2010).

© Universiti Teknikal Malaysia Melaka

2.6 Summary

Osteoarthritis is a common joint disease among elderly. The main cause is degeneration of the articular cartilage. Articular cartilage is a fine connective tissue that cover the extremity of the articulating bone in synovial joint. OA begins with the proteolytic breakdown of the cartilage matrix, the fibrillation and erosion of the cartilage surface and the beginning of the synovial inflammation. In the early stage of OA, decreasing of the biomechanical properties are significant. There are some treatments help to relieve the symptom and does not get worse. However, there is no cure for OA. Therefore, it is important to study in determination of structural, composition and biomechanical properties of the cartilage for early identification of disease.

Non-invasive imaging techniques are common method for revealing the structure, composition and pathology of articular cartilage. There are various imaging techniques including magnetic resonance imaging (MRI), X-ray, ultrasound and arthroscopy. However, MRI is widely used to visualize the cartilage because it provides high resolution image in short time.

UNIVERSITI TEKNIKAL MALAYSIA MELAKA

From the previous studies, high field MRI was used to examine the properties of the cartilage (Gudbergsen et al., 2012, Calvo et al., 2001, Luke et al., 2010). In this study, low field MRI was used to determine the correlation between MRI image greyscale and biomechanical properties.

© Universiti Teknikal Malaysia Melaka

CHAPTER 3

METHODOLODY

This chapter describe the methodology used in this project to characterise the MRI image greyscale and biomechanical properties on different water content of cartilage. This project starts by conducting the creep indentation test to determine the deformation of the cartilage tissue. Finite element model was developed using ABAQUS software. From the simulation data of finite element model and incorporation with the experimental data, the biomechanical properties of the articular cartilage is obtained. Greyscale of MRI images were determined to study the correlation with the biomechanical properties of the cartilage. Figure 3.1 shown the flow chart of the project.

UNIVERSITI TEKNIKAL MALAYSIA MELAKA

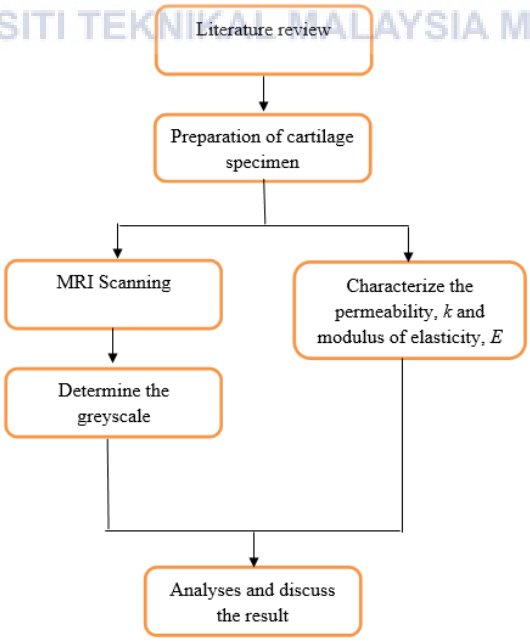

Figure 3.1: Flow chart of the methodology.

© Universiti Teknikal Malaysia Melaka

3.1 Material and Specimen Preparation

3.1.1 Phosphate Buffered Saline

Phosphate buffered saline (PBS) is a solution that contains sodium chloride, disodium phosphate, potassium chloride and monopotassium phosphate. Chemical composition of 1.0 mol/L PBS has a final concentration of 137 mN sodium chloride and 2.7 mmol/mM potassium chloride (www.thoughtco.com). It has pH value ranged from 7.2 to 7.6 (www.bosterbio.com). It is prepared by dissolved the PBS tablet in the distilled water with the ratio of 1 tablet in 100 ml of distilled water. The cartilage specimen is soaked in PBS throughout the experiment to develop a similar cartilage physiological in situ. Figure 3.2 shown the PBS tablets dissolved in the distilled water.

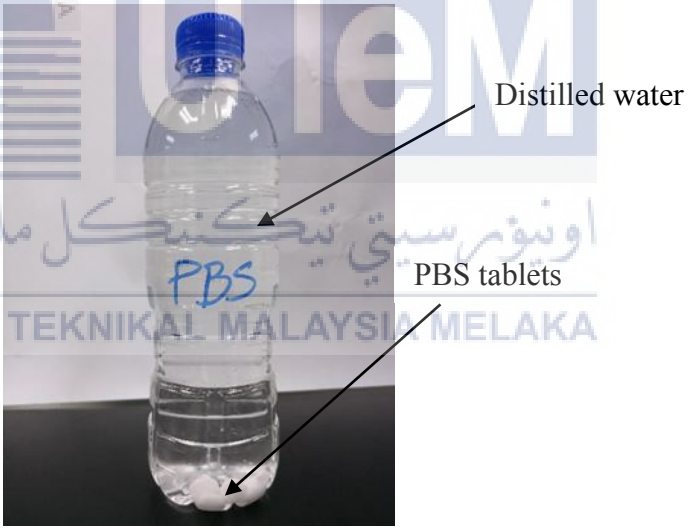

Figure 3.2: Preparation of PBS.

© Universiti Teknikal Malaysia Melaka

3.1.2 Specimen Preparation

The specimen used in this research is the articular cartilage of bovine femoral head of hip joint. The bovine hip joint bought from the local abattoir in Jasin. The flesh is removed by using scalpel. Then, the joint is cut out by using electric handsaw. The excess tissues and damaged surfaces are removed. After that, the joint cut into slices and drill out the small piece of bone that attached the cartilage by using electric hand drill. The bone is removed by using scalpel. The cartilage specimen were prepared and soaked in the phosphate buffered saline (PBS) to prevent dehydration. Figure 3.3(a) shown the bovine femoral head of hip joint after processed.

The specimens were put at the room temperature which is 25 ºC to dehydrate. Every 30 minutes, the specimens were weighted using analytical balance. Figure 3.3(b) shown the specimens put in the room temperature to dehydrate. After that, the percentage of the water content in the specimen is calculated. Similar method was used in previous study to drying the cartilage specimens (Berberat et al., 2009). After long time exposed to air, the cartilage specimens become yellow, rough and loses its glossy appearance. This resulted the cartilage's tissue drying, chondrocytes death and extracellular matrix altering (Paterson et al., 2015).

UNIVERSITI TEKNIKAL MALAYSIA MELAKA

The percentage of water content is calculated by the formula (Hannafin and Arnoczky, 1994):

$$Percentage\ of\ water\ content = \frac{Wet\ weight - Dry\ weight_{0,30,60,90}}{Wet\ weight} \text{x}100\%$$

© Universiti Teknikal Malaysia Melaka

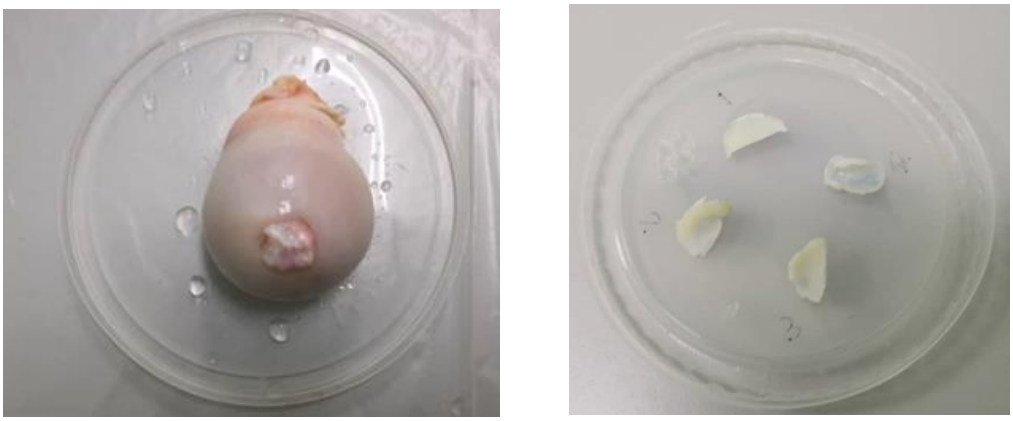

(a) (b)

Figure 3.3: (a) Bovine femoral head (b) specimens put in the room temperature to dehydrate.

3.2 Magnetic Resonance Imaging

The scanning of the specimens were performed on a 0.18 T low-field MRI Esaote C-scan machine. The MRI systems consists of three main parts that are computer system, patient table and magnetic unit scanner. The main advantages of the low-field extremity scanner are low maintenance cost and space saving compared to high-field scanner. It requires a constant 110 volt outlet for input. Figure 3.4 shown the MRI scanner in the present used.

© Universiti Teknikal Malaysia Melaka

(a) (b)

Figure 3.4: The C-scan MRI system (a) outer look (b) coil used.

In order to calibrate the MRI system, it requires to scan a phantom to examine the homogeneity of the generated image. Figure 3.5(a) shown the phantom that filled with fluid in a container in present study. The phantom was scanned with gradient echo (GRE) sequence. Figure 3.5(b) shown the image captured by the MRI system.

UNIVERSITI TEKNIKAL MALAYSIA MELAKA

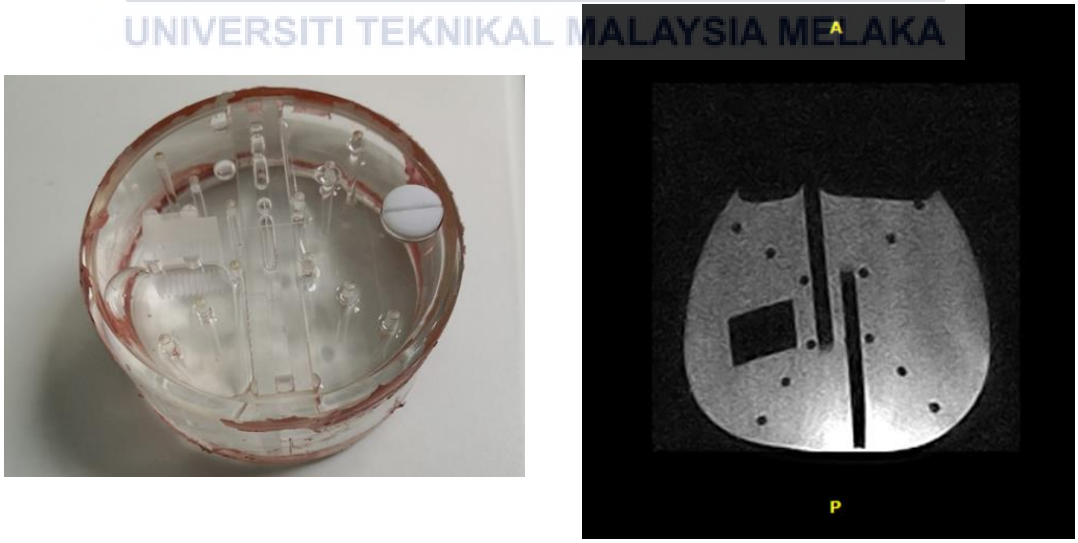

(a) (b)

Figure 3.5: (a) Imaging phantom (b) MR image of imaging phantom

© Universiti Teknikal Malaysia Melaka

3.2.1 MRI Image Acquisition for Cartilage

The scan was performed within 48 hours after slaughter in order to make sure the specimens were in optimal condition. The specimens were put on the phantom while scanning because the specimens were too small for scanning. Each specimens was placed axially at the center of the receiving coil inside the scanner as shown in Figure 3.6. The surface of the cartilage was exposed to yield a better image of the tissue. The specimen was scanned in three planes which were coronal, sagittal and transverse. After that, the specimens were scanned using the standard imaging sequence available in the low-field MRI which was gradient echo.

UNIVERSITI TEKNIKAL MALAYSIA MELAKA

Figure 3.6: Specimens placed in the receiving coil.

3.2.2 MRI Image Processing

The MRI image generated were in standard DICOM (Digital Imaging and Communication in Medicine) format. The images were processed using Matlab software V 7.12.0 R 2011a (MathWorks Inc., MA, USA). The image will be characterised based on the intensity of the greyscale in every pixel in order to correlate with biomechanical

© Universiti Teknikal Malaysia Melaka

properties by using custom written Matlab program. Matlab commands in the explanatory list can be found in Appendix A.

3.2.3 Characterisation of the MRI Image

Greyscale is a range of number correlated with the image pixel charactering the shade of white, grey and black. In this study, MRI images were utilised to study the features of articular cartilage based on the image greyscale. The greyscale resolution of the MRI image in the present study is in 16-bits per pixel allocation, which resulted in the greyscale intensity from 0 to 65,536 while the maximum bit stored is 12-bits. In order to determine the greyscale, a rectangular region of interest (ROI) was selected in the centre of the cartilage specimen where indentation test was exactly conducted. The ROI consisted of 9 pixels (3x3 pixels) consistent engagement of cartilage across the thickness of cartilage as shown in Figure 3.7. The cartilage greyscale of the exact area was determined by averaging the 9 pixels.

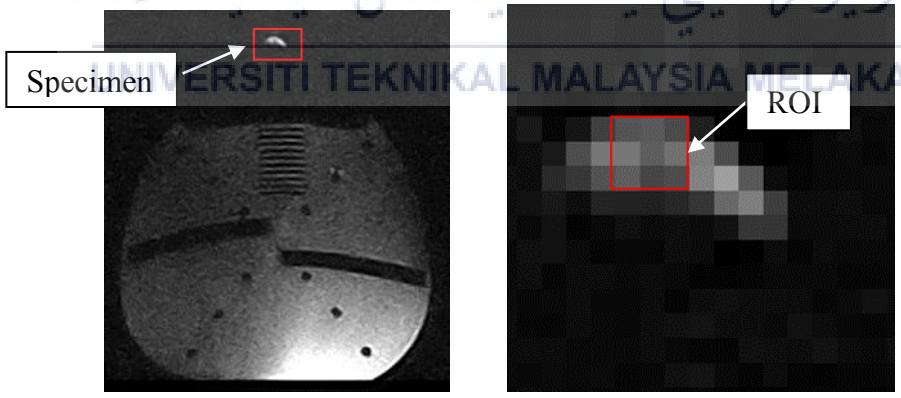

(a) (b)

Figure 3.7: (a) MRI image of the articular cartilage from gradient echo sequence (b) Close view of the MRI image and cropped image

© Universiti Teknikal Malaysia Melaka

3.3 Experimental Method

The experiment method in this study consists of cartilage thickness measurement and creep indentation test. The value of thickness of the cartilage were used to develop the finite element model. The experimental data was obtained from the creep indentation test to characterize the biomechanical properties of the cartilage such as elastic modulus and permeability by merging the result with the computational simulation. Elastic modulus is the measurement of the stiffness of the tissue whereas the permeability is the resistance of the fluid flow. Indentation test was used in previous studies because it involved only simple experiment procedure with the combination of experimental and computational method to derive the equilibrium elastic modulus and permeability of cartilage

3.3.1 Indentation Test

The indentation test was carried out on the cartilage specimens to study the time-dependent and the deformation response of the cartilage. From these results, the biomechanical properties of the articular cartilage can be characterize. The custom-made indenter apparatus is used to perform the indentation test. The indentation test rig made up by several main components, for example, linear variable differential transformer (LVDT), force transducer connected with a shaft, spherical indenter and specimen holder. Figure 3.8 shown the indenter apparatus used in present study.

© Universiti Teknikal Malaysia Melaka

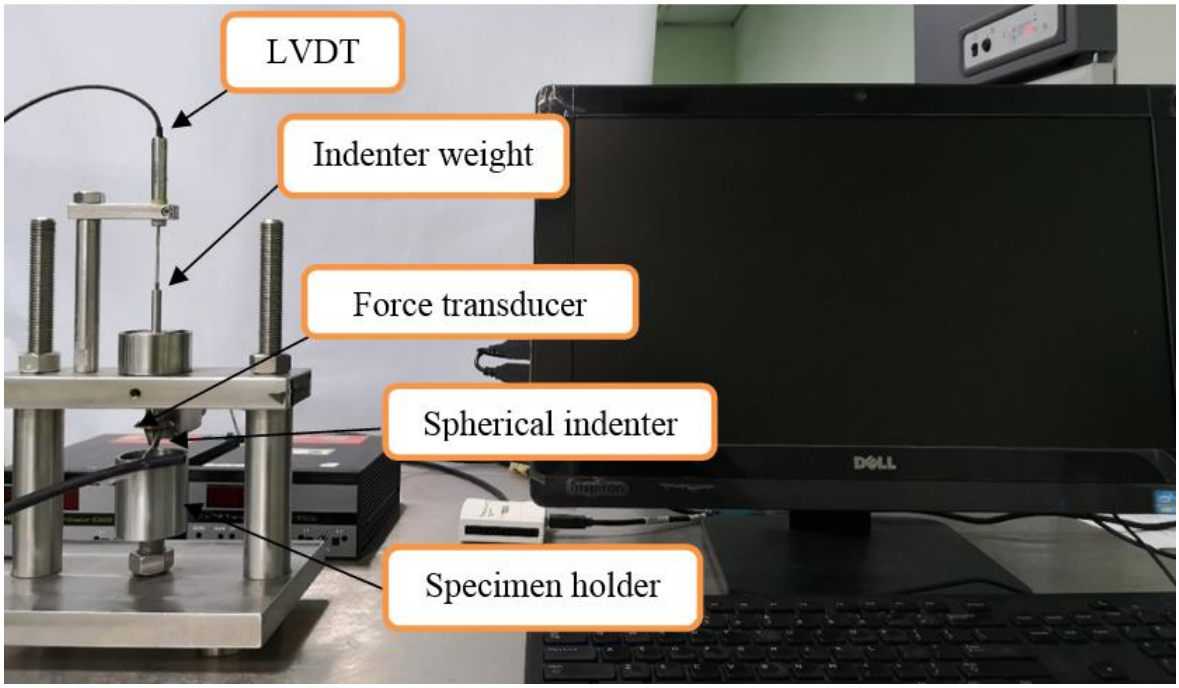

Figure 3.8: Indenter apparatus.

The force transducer connected to a shaft at its upper end and a 4 mm diameter spherical indenter at its lower end. The function of the force transducer is to detect the force when the indenter pressed on the cartilage surface. At the same time, the monitoring of the displacement of the shaft and recording the deformation on the cartilage surface are by LVDT. The total weight of the force transducer assembly is 0.38 N. The data from LVDT and force transducer were shown at the digital display and data acquisition. These data were stored into computer using LabVIEW 8.5.1 software.

UNIVERSITI TEKNIKAL MALAYSIA MELAKA

3.3.2 Calibration Procedure

The calibration of the LVDT transducer was carried out before creep indentation test to test the reliability of the apparatus and to obtain the calibration factor for the displacement. Figure 3.11 shown the calibration of the LVDT transducer.

© Universiti Teknikal Malaysia Melaka

(a)

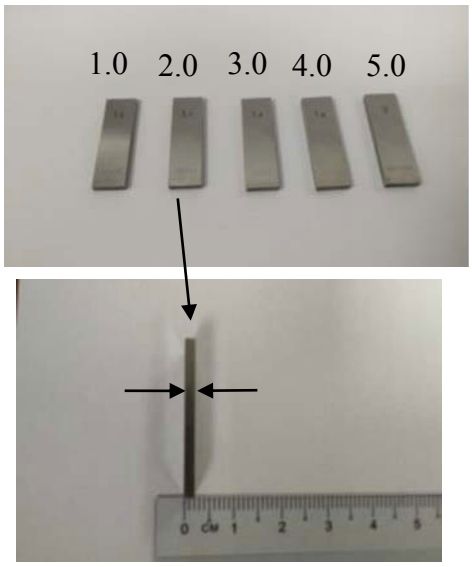

(b)

Figure 3.9: Procedure of the calibration test. (a) Set-up of the calibration test (b) Different height of stainless steel gauge blocks.

Stainless steel block gauges were used to calibrate the displacement data measured from the LVDT transducer. The indenter was released on the gauge block at different height as shown in Figure 3.9 (b). The weight of shaft was maintained while the differences in the output voltage from the LVDT were recorded during the addition or removal of the block gauges during the process. This step was repeated three times to attempt the average value and to evaluate the repeatability of the measurement. During the test, the calibration factor was used to convert the value of the displacement data from voltage to millimetre units. Figure 3.10 shown the linear regression fit of plotting of the displacement of the indenter onto the gauge surface.

UNIVERSITI TEKNIKAL MALAYSIA MELAKA

© Universiti Teknikal Malaysia Melaka

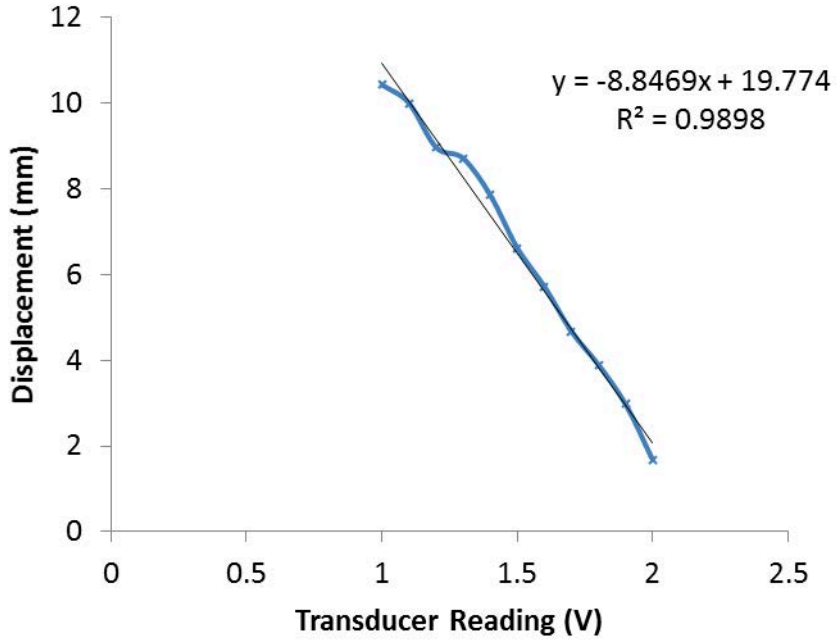

Figure 3.10: Graph represents the measurement taken in the load calibration.

3.3.3 Creep Indentation Test

Creep indentation test was carried out to provide the deformation and time data. The biomechanical properties of the cartilage can be characterized from the data of test. The specimens fitted in the specimen holder to prevent any movement during the test. Figure 3.11 shown the creep indentation test rig used to perform creep indentation test.

© Universiti Teknikal Malaysia Melaka

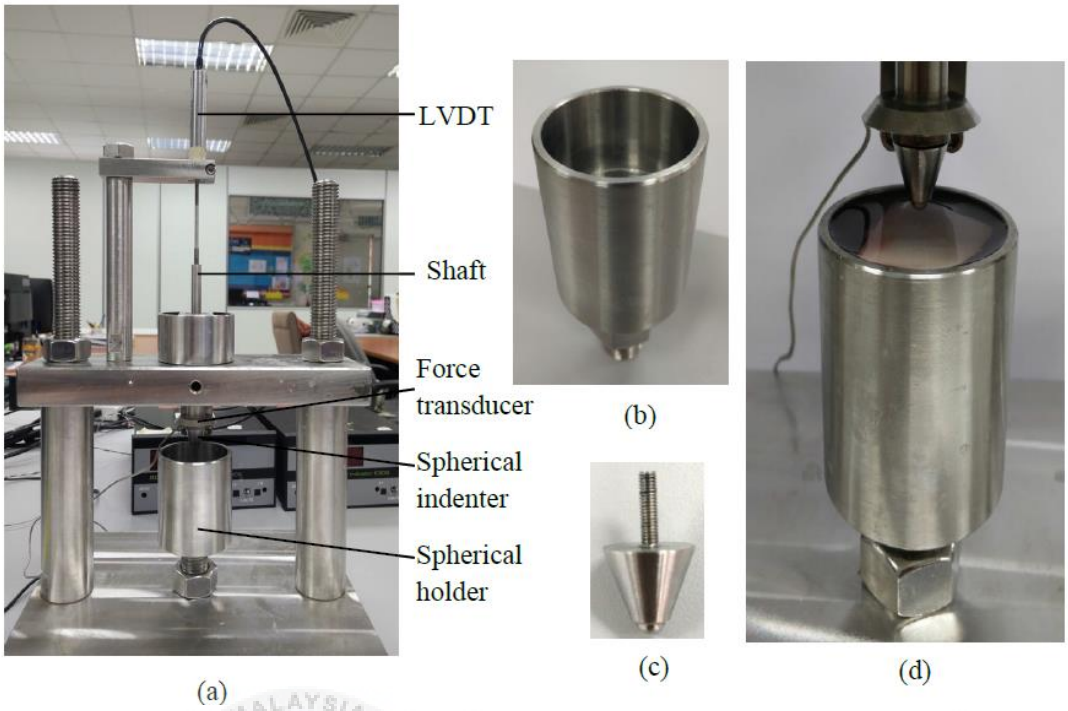

Figure 3.11: Apparatus for creep indentation test (a) Components of the test rig (b) Specimen holder (c) 4 mm diameter of the spherical indenter (d) Closer view in the indented specimen.

The test was conducted using a 4 mm diameter spherical indenter. The indenter was adjusted near to the cartilage surface to make sure the load indicator has contact with the cartilage surface. The compressive force acting on the cartilage was 0.38 N. The indenter was then released and the displacement of the cartilage specimen was recorded continuously at sampling time of 0.01 seconds for 1000 seconds by which the displacement had reached the equilibrium state. All the data were saved using data acquisition software, LabVIEW.

UNIVERSITI TEKNIKAL MALAYSIA MELAKA

© Universiti Teknikal Malaysia Melaka

3.3.4 Cartilage Thickness Measurement

The measurement of the cartilage thickness was conducted to determine the cartilage properties characterised according to the specific thickness in the finite element model. The thickness was measured using a profile projector, SeDOz-G XTR microprocessor profile projector (model: JT12A0. Profile projector is an optical instrument used to measure the dimension or the radii of the object or hole position. The profile of the object is magnified by the projector and displayed in the projection screen.

In the present study, the specimen was placed on the glass table using adhesive clay to fix the specimen in place throughout the measurement. The measurement was performed on each specimen with respective points as shown in Figure 3.12. The points were marked on the edge of the cartilage to measure the thickness. The step was repeated for three times to attain the consistent reading.

UNIVERSITI TEKNIKAL MALAYSIA MELAKA

Figure 3.12: Measurement of the cartilage thickness using profile projector.

© Universiti Teknikal Malaysia Melaka

3.4 Computational Method

Computational method was incorporated with creep indentation test results to characterize the cartilage biphasic properties. These cartilage biphasic properties included permeability, *k* and modulus of elasticity, *E*. ABAQUS 6.9 software was used to create an axisymmetric biphasic poroelastic finite element model to characterize the properties of the cartilage.

3.4.1 Verification of Finite Element Model

To verify the contact-dependent flow algorithm, the model which was developed by Pawaskar (2010) was reconstruct. The interface and boundary condition, element types, and cartilage properties used were same. The contact-dependent algorithm can evaluate the flow condition between free surface and the contact moment region of the indenter with the cartilage surface.

UNIVERSITI TEKNIKAL MALAYSIA MELAKA

An axisymmetric model with a 3 mm and 20 mm radius of cartilage and a rigid spherical indenter of 5 mm was established. The model consisted of 3200 (200×16) four-node bilinear displacement and pore pressure, reduced integration with hourglass control (CAX4RP) elements. For the boundary condition, the bottom nodes of the cartilage were constrained in both horizontal and vertical directions, while the nodes on the axis were constrained in horizontal direction. The spherical indenter was only allowed to move in vertical direction. The pore pressure on the nodes of the outer edge was remained at zero so to allow the unrestricted fluid flow. The cartilage surface that contact with the indenter was set as the contact-dependent flow. No fluid flow was set at the bottom surface and vertical symmetry axis to restrict the fluid flow. Figure 3.13 shown the axisymmetric finite element model used in the simulation of the compression test.

© Universiti Teknikal Malaysia Melaka

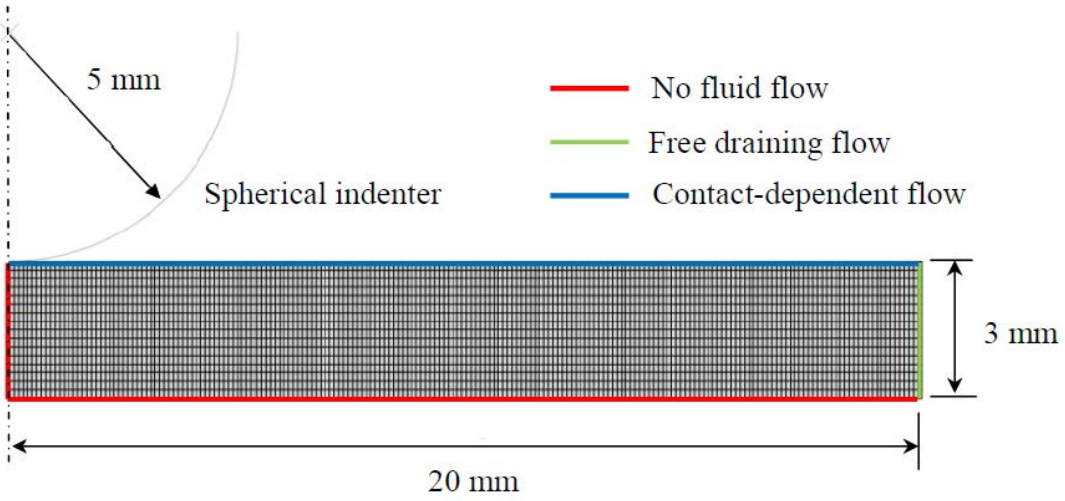

Figure 3.13: Axisymmetric finite element model for contact-dependent flow of articular cartilage with a rigid spherical indenter (Pawaskar et al., 2010).

The creep-deformation simulation was conducted by applying a ramp load of 0.9 N on the indenter for 2 seconds with the load maintained for a further 1000 seconds. Table 3.1 shown the properties applied on the cartilage in previous study.

UNIVERSITI TEKNIKAL MALAYSIA MELAKA

© Universiti Teknikal Malaysia Melaka

Table 3.1: Cartilage properties of articular cartilage for finite element verification model. (Pawaskar et al., 2010).

Parameter	Value
Young's modulus, E	0.54 MPa
Poisson's ratio, v	0.08
Permeability, k	4.0×10^{-15} m^4/Ns
Void ratio, e	4.0 (80 % interstitial fluid)

In order to verify the contact-dependent flow algorithm, the verification of the FE model was carried out. Based on the contact stress at the cartilage surface nodes, contact-dependent flow algorithm was developed to change the flow conditions. Figure 3.14 and 3.15 shown the identical result generated in the present developed model for both contact pressure and pore pressure compared to the result generated by Pawaskar (2010). The implementation of the contact-dependent algorithm was confirmed.

UNIVERSITI TEKNIKAL MALAYSIA MELAKA

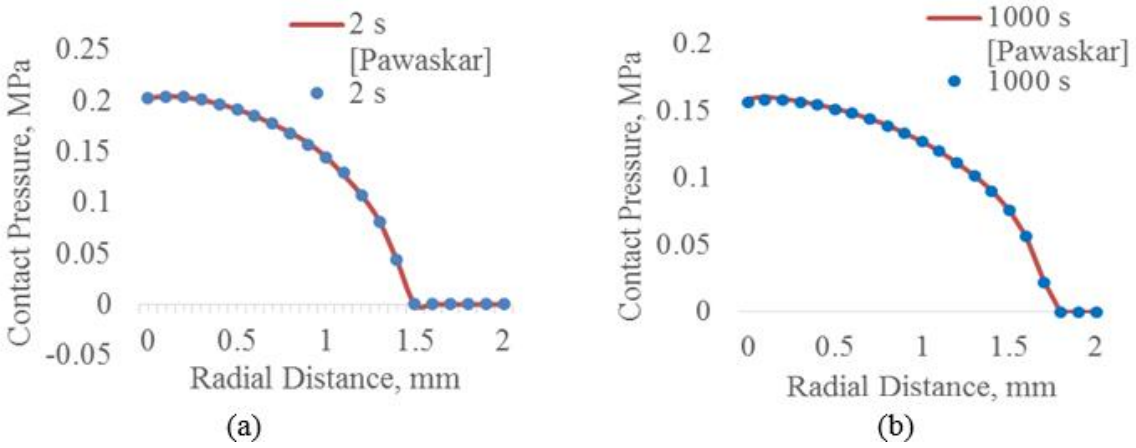

Figure 3.14: Contact pressure distribution on cartilage surface at (a) 2 seconds (b) 1000seconds

© Universiti Teknikal Malaysia Melaka

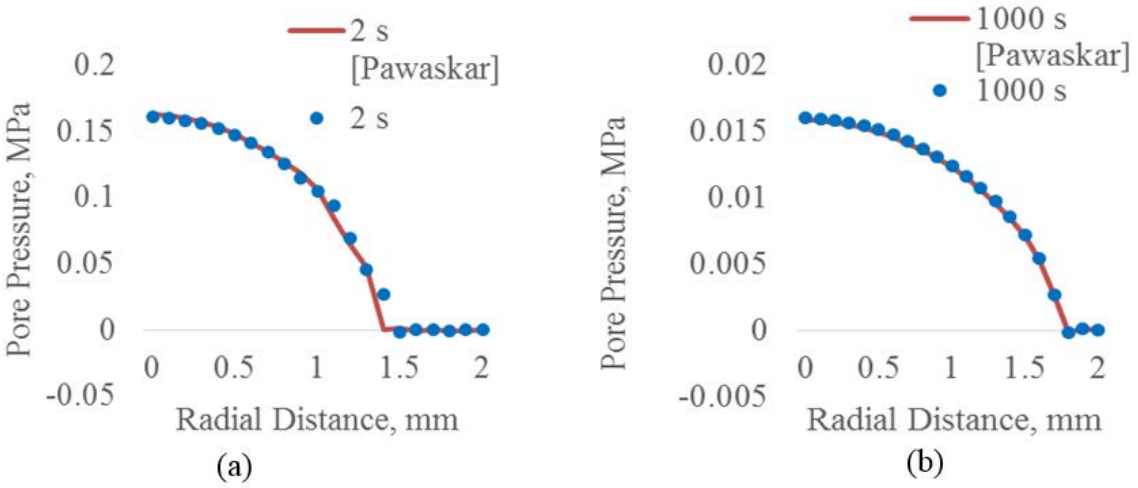

Figure 3.15: Pore pressure distribution on the cartilage surface for (a) 2 seconds (b) 1000 seconds

3.4.2 Development of Finite Element Model

In order to determine the linear biphasic properties, the articular cartilage was modelled as axisymmetric biphasic poroelastic element. The finite element model was developed using measured thickness and diameter with 1.297 mm and 4 mm width. The spherical indenter of a 4 mm diameter was modelled as an analytical rigid surface. Figure 3.16 shown the FE model for the cartilage and the spherical indenter.

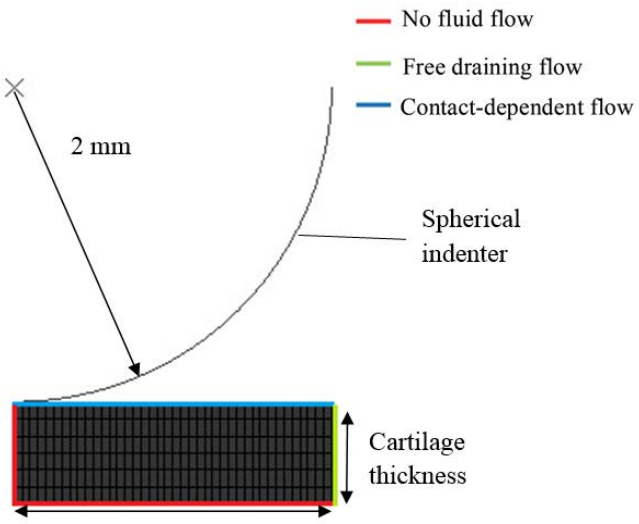

Figure 3.16: Axisymmetric FE model of the cartilage specimen.

© Universiti Teknikal Malaysia Melaka

Four-node bilinear displacement and pore pressure elements (CAX4P) were used to model the element type for the cartilage. For simulation of the experimental creep indentation test, the boundary and interface condition were applied on the FE model. For the boundary condition, the nodes on the axis were constrained in the horizontal direction, while the bottom nodes were constrained in both horizontal and vertical directions. The spherical indenter was only allowed to move in the vertical direction.

The contact-dependent flow condition was applied at the top of the cartilage. The fluid flow was prevented at the bottom and the vertical symmetry axis of cartilage surface. For the outer edge, the nodes were maintained at zero pore pressure to allow the unrestricted fluid flow. The material properties of the articular cartilage applied in the finite element models were tabulated in Table 3.2.

Table 3.2: Material properties for the finite element model (Pawaskar, 2010).

Parameter	Value
Young's Modulus, E	0.54 MPa
Poisson's ratio, ν	0.08
Permeability, k	4.0×10^{-15} m^4/Ns

Based on the indenter test experiment, a ramp load of 0.38 N was applied on the spherical indenter for two seconds. In order to simulate the creep deformation phenomenon, the load was then maintained at 0.38 N for a further 1000 seconds. The 2 seconds ramp period was based on the experimental studies as an instantaneous effect, which found that the minimum time at which the creep indentation test of the cartilage could be compared reliably after the application of load (Pawaskar et al., 2010).

© Universiti Teknikal Malaysia Melaka

3.5 Characterisation of Cartilage Biomechanical Properties

The biomechanical properties included elastic modulus and permeability were characterised by the results from a combination of experimental and computational methods. An axisymmetric biphasic poroelastic finite element model was carried out to simulate the experimental creep indentation test conducted on the cartilage specimens. The cartilage biphasic biomechanical properties of elastic modulus and permeability were characterised by fitting the cartilage deformation curve generated from the FE model to the experimental deformation curve by sequentially tuning these properties as shown in Figure 3.17. The red circles represent the data from the experimental curve produced during the indentation test whereas the blue line represents the graph produced by the FE model. The parameter values were altered until the deformation time curve implemented from the FE model fitted to the experimental data after iteratively changing the properties of FE. A non-linear least-square method was used to generate the curve-fitting by the 'Isqnonlin' function in Matlab software (V7.12.0 R2011a, MathWorks Inc, MA, USA) followed the method developed by Pawaskar (2010). In order to minimize the sum of the least square error, curve fitting was taken. The resulting elastic modulus and permeability were taken as the biomechanical properties of the individual cartilage specimen after the curve fitting. The initial values of elastic modulus and permeability were used to initiate the iteration whereas the final optimised values were obtained when the function achieved the minimal squared error occurred or minimum specified convergence criteria between the curves. Automatic time increment with UTOL parameter, which specified the allowed maximum change in pore pressure in one increment at 600 kPa was used to produce acceptable results. Figure 3.17 shown an example of the cartilage deformation curve.

© Universiti Teknikal Malaysia Melaka

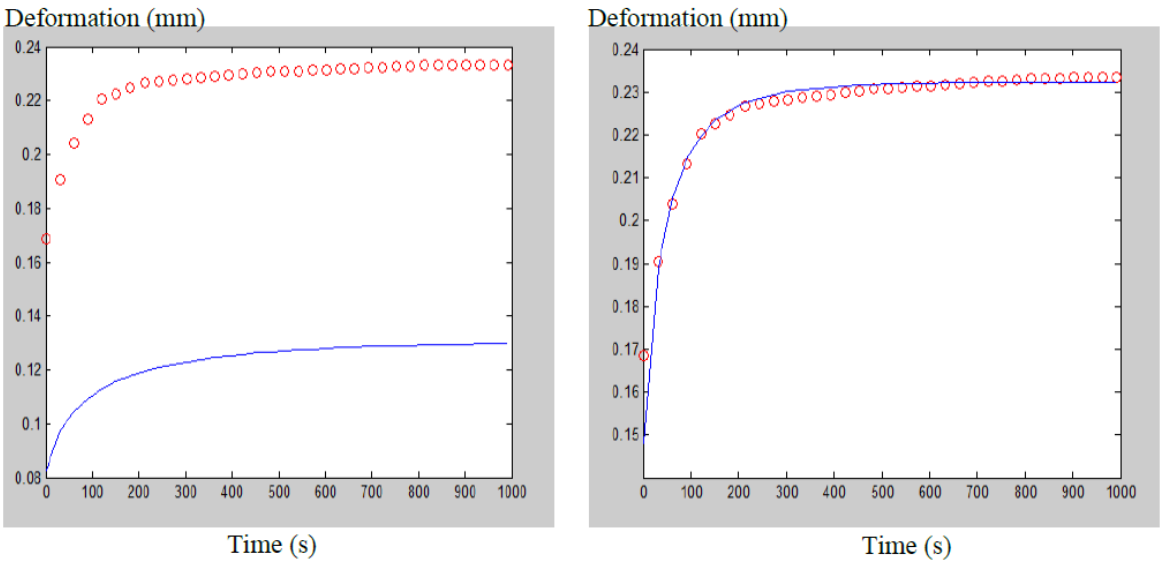

Figure 3.17: Cartilage deformation curve.

3.6 Statistically Analysis

All data are presented as average ± standard deviation. In order to determine the relationships between the MRI image greyscale and the biomechanical properties of the cartilage, Linear Pearson correlation coefficient was used. The linear correlation coefficient, r was used to study the relationship between cartilage greyscale and biomechanical properties. The formula for the linear Pearson correlation coefficient, r is as below:

$$r = \frac{\Sigma(X-\bar{X})(Y-\bar{Y})}{\sqrt{(X-\bar{X})^2(Y-\bar{Y})^2}}$$

© Universiti Teknikal Malaysia Melaka

CHAPTER 4

RESULTS AND DISCUSSION

This chapter presents the result and analysis of the study. The first section shows the effect of dehydration on water content. The second section is the effect of dehydration on MRI greyscale. Third section details the thickness of the articular cartilage. The biomechanical properties of the articular cartilage were characterised using a combinational of creep indentation test and computational axisymmetric finite element model methods. After that, the correlation of biomechanical properties and MRI greyscale were presented in the final section.

UNIVERSITI TEKNIKAL MALAYSIA MELAKA

4.1 The Effect of Dehydration on Water Content

Figure 4.1 shown the percentage of water content in cartilage specimens at initial, 30 minutes, 60 minutes and 90 minutes exposed in room temperature. It was found that the percentage of water content in cartilage specimens decreased with time. In this study, the average percentage of water content at fresh condition was 76.8 ± 4.5%. The water content of the fresh articular cartilage was within the range of 70-80% (Xu et al., 2011). At 30 minutes, the percentage of water content reduced to 72.9 ± 6.1% and reached to 57.9 ± 12.6% at 90 minutes. In addition, the water loss 15.0 ± 18.7% from 30 minutes to 90

© Universiti Teknikal Malaysia Melaka

minutes. From the previous study, it was found that the water content decreased with time when the specimens put at the humid environment (Maroudas, 1977).

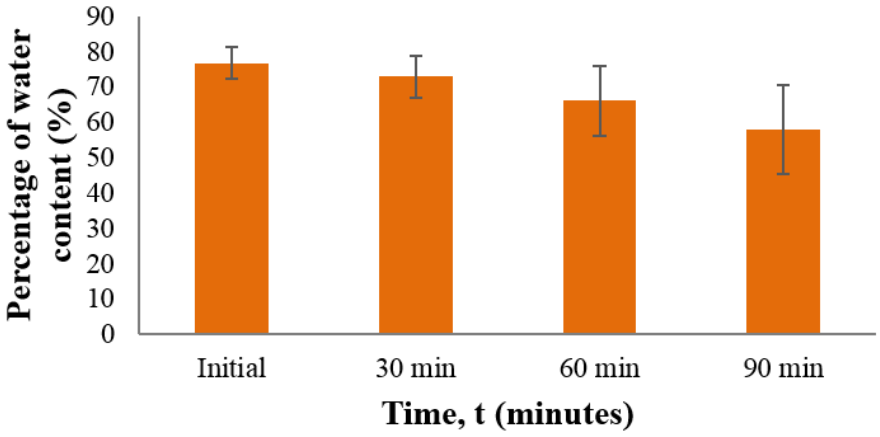

Figure 4.1: Percentage of water content against time.

4.2 The Effect of Dehydration on MRI Greyscale

Figure 4.2 shown the MRI image greyscale of the cartilage specimens against time. It was found that the greyscale value decreased with time. In this study, the average value of the greyscale value at fresh condition was 2201.3 ± 241.3. At 30 minutes, the greyscale value reduced to 1879.5 ± 387.7 and reached to 1398.8 ± 407.2 at 90 minutes. Furthermore, the greyscale value decreased 480.7 ± 794.9 from 30 minutes to 90 minutes. It was found that the higher the water content, the higher the MRI image greyscale of the cartilage (Wansin et al., 2017).

UNIVERSITI TEKNIKAL MALAYSIA MELAKA

© Universiti Teknikal Malaysia Melaka

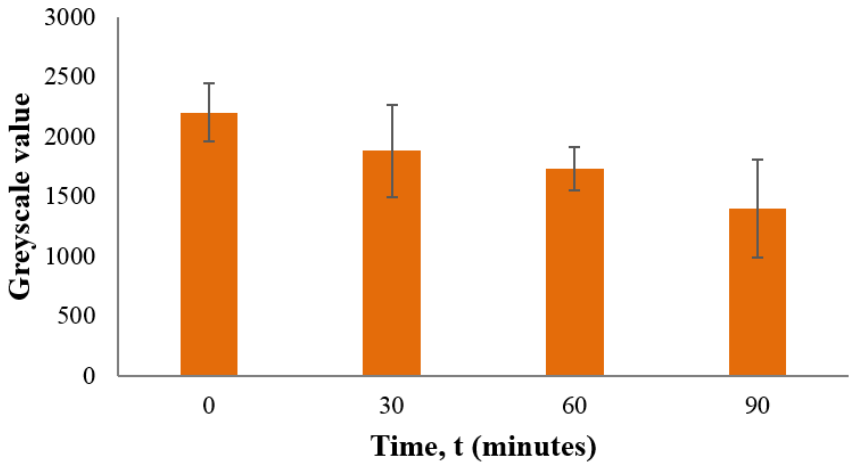

Figure 4.2: Greyscale of cartilage specimens against time.

4.3 Thickness Measurement

Thickness measurement is important as to develop the finite element model. In the present study, the average thickness of the cartilage sample is 1.297 ± 0.251 mm. From the previous studies, the thickness of the femoral head cartilage is in the range of 0.800 mm to 1.600 mm. Table 4.1 shown the thickness of cartilage specimens in present study and previous studies.

UNIVERSITI TEKNIKAL MALAYSIA MELAKA

Table 4.1: Thickness of cartilage specimens.

Cartilage	Thickness, mm	Reference
Femoral head	1.297 ± 0.251	Present study
Patellofemoral	1.430 ± 0.140	Chen et al. 2001
Humeral head	0.800-1.600	Niinima et al. 2001

© Universiti Teknikal Malaysia Melaka

4.4 The Effect of Dehydration on Biomechanical Properties

The biomechanical properties of the articular cartilage are important in determine the degeneration and function of the tissue. The experimental and computational data were used to characterise biphasic properties of elastic modulus, E and permeability, k of articular cartilage. The data from experimental and computational methods were compiled to generate a deformation graph using Matlab software (Pawaskar et al., 2010).

From the results, it was found that elastic modulus, E increased as the cartilage exposed for long time as shown in Figure 4.3. The average elastic modulus of the initial condition was 0.39 ± 0.14 MPa. After 30 minutes, the elastic modulus increased to 0.71 ± 1.11 MPa and reached to 2.51 ± 0.51 MPa at 90 minutes. The elastic modulus had increased 550.91% from initial to 90 minutes. This trend also found in previous studies. The elastic modulus decreased as the water content of the cartilage increased (Armstrong and Mow, 1982, Mow et al.,1984). Based on previous studies, the elastic modulus of the articular cartilage at fresh condition was in the range of 0.02 to 1.01 MPa as shown in Table 4.3. It is expected the cartilage specimens at 90 minutes have the highest elastic modulus. This is because there is less solid matrix especially proteoglycan when the water content is higher (Armstrong and Mow, 1982).

UNIVERSITI TEKNIKAL MALAYSIA MELAKA

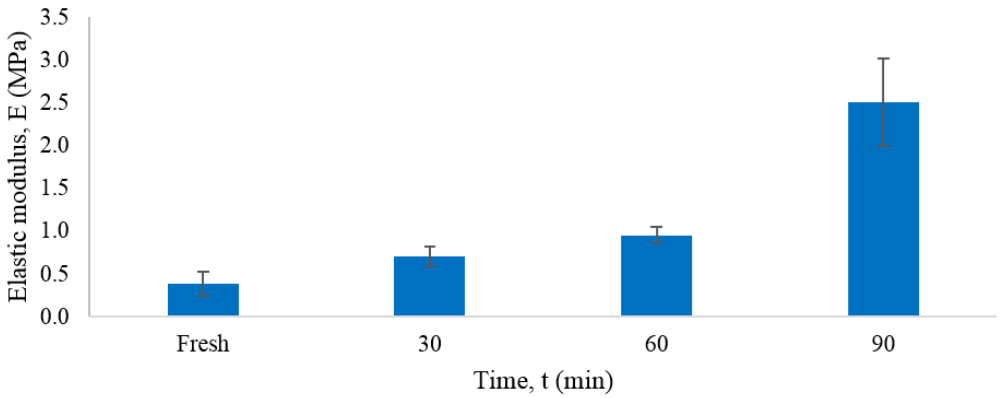

Figure 4.3: Elastic modulus, E at fresh condition, after 30 minutes, 60 minutes and 90 minutes exposed at room temperature.

© Universiti Teknikal Malaysia Melaka

Table 4.2: Elastic modulus in present and previous study.

Cartilage	Technique	Elastic modulus, E (MPa)	Reference
Femoral head	Indentation	0.39 ± 0.13	Present study
Humeral head	Confined compression	1.01 ± 0.42	Ph et al. 2006
Patellofemoral	Indentation	0.7 ± 0.09	Armstrong 2013
Talus	Confined and unconfined compression	0.02 ± 0.8	Ms and Bs 2009

UNIVERSITI TEKNIKAL MALAYSIA MELAKA

Figure 4.4 shown the permeability of cartilage specimens at initial, 30 minutes, 60 minutes and 90 minutes exposed in room temperature. It was found that the permeability of cartilage specimens decreased with time. In present study, the average permeability of cartilage at fresh condition was $22.59 \pm 14.85 \times 10^{-15}$ m^4/Ns. After 30 minutes, the permeability decreased to $2.30 \pm 0.42 \times 10^{-15}$ m^4/Ns and reached to $1.51 \pm 0.51 \times 10^{-15}$ m^4/Ns at 90 minutes. This trend also found in previous study. This is due to as the water content increases, the permeability of the cartilage increases because the matrix of tissue become softer (Armstrong and Mow, 1982).

© Universiti Teknikal Malaysia Melaka

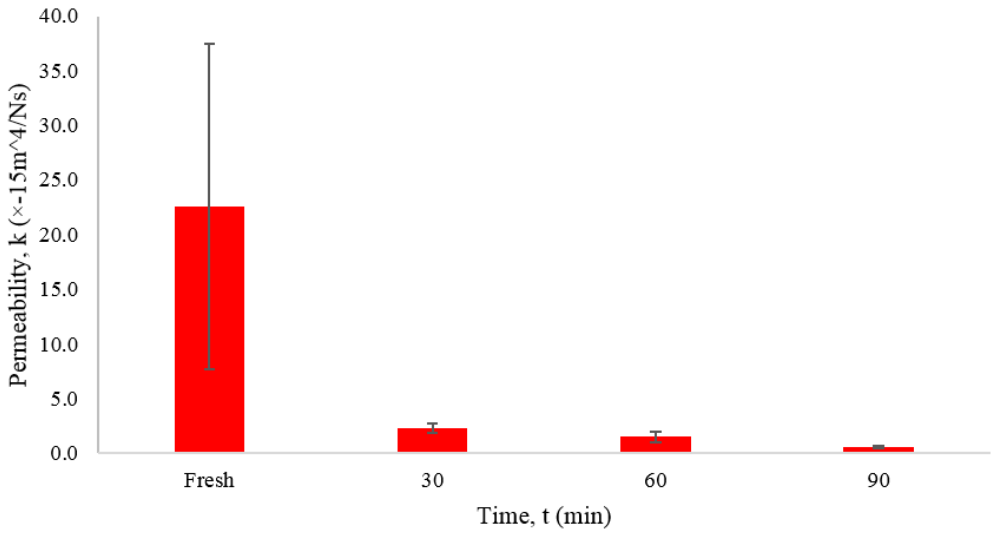

Figure 4.4: Permeability, *k* at fresh condition, after 30 minutes, 60 minutes and 90 minutes exposed at room temperature.

UNIVERSITI TEKNIKAL MALAYSIA MELAKA

4.5 Correlation of Biomechanical Properties and MRI Greyscale

To study the relationship between the MRI image greyscale and the biomechanical properties of the cartilage specimen, Linear Pearson correlation analysis was performed. Figure 4.5 and 4.6 shown the Linear Pearson correlation of biomechanical properties and MRI greyscale.

It was found that a decrease of the elastic modulus resulted in an increment in the greyscale value that created a moderate correlation (r = -0.617). On the other hand, there is an increase of the permeability resulted in an increment in the greyscale value and create a moderate correlation also (r = 0.593).

© Universiti Teknikal Malaysia Melaka

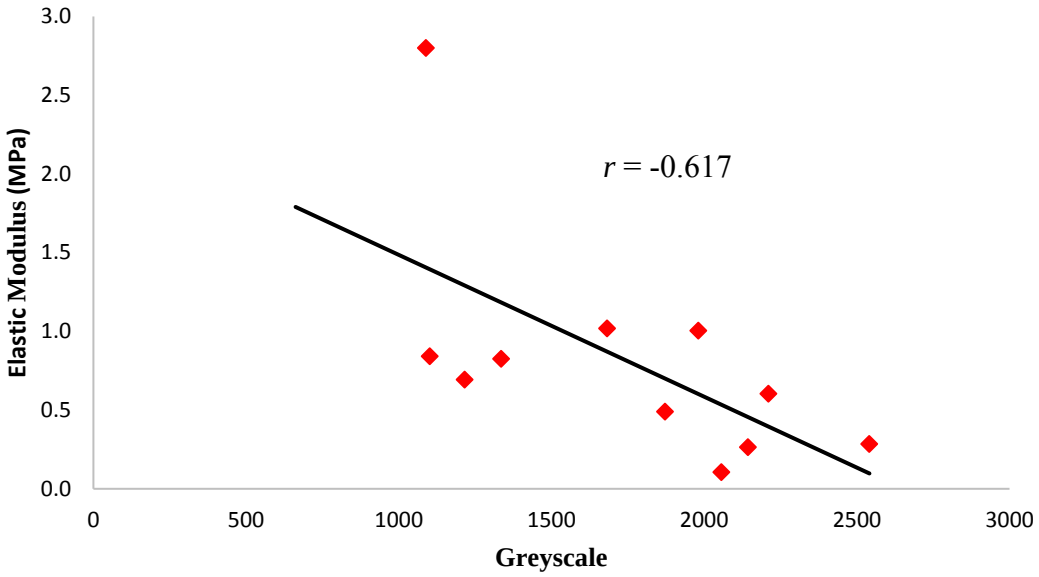

Figure 4.5: Linear Pearson correlation of elastic modulus and greyscale of the cartilage.

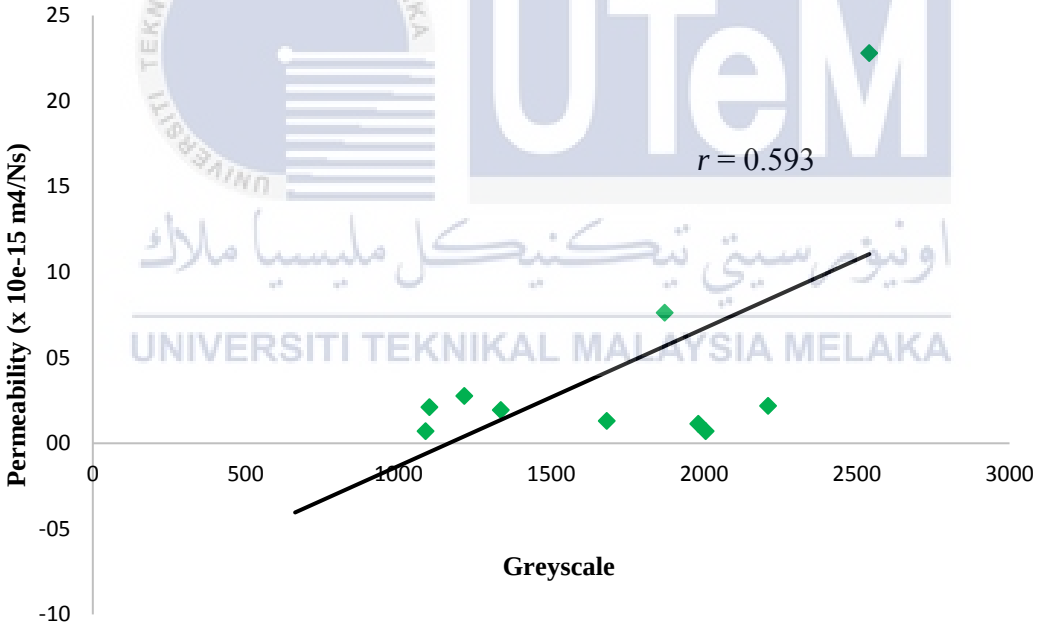

Figure 4.6: Linear Pearson correlation of permeability and greyscale of the cartilage.

Linear Pearson correlation analysis was used to study the relationship between the MRI image greyscale and biomechanical properties of the cartilage. There were similar

© Universiti Teknikal Malaysia Melaka

analyses to investigate between the quantitative MRI imaging and biomechanical properties of the cartilage (Blumenkrantz and Majumdar, 2007, Nieminen, 2004).

From the present result, moderate correlations were obtained between the low field MRI image greyscale and biomechanical properties of the articular cartilage. The *r* values for elastic modulus was 0.617 and permeability was 0.593. The correlation between greyscale and cartilage elastic modulus was slightly higher compared to the correlation between greyscale and cartilage permeability. This could be because the water content contributes up to 80% of wet weight of articular cartilage. It was found that the elastic modulus dependent on the water content of the articular cartilage (Lu and Mow, 2008).

UNIVERSITI TEKNIKAL MALAYSIA MELAKA

© Universiti Teknikal Malaysia Melaka

CHAPTER 5

CONCLUSION AND RECOMMENDATION

5.1 Conclusion

This study was conducted to the effects of water content on biomechanical properties and MRI image of articular cartilage. The MRI unit used in this study was low field extremity scanner.

In this study, the low field 0.18 T MRI was utilised to study the cartilage greyscale using gradient echo imaging sequence. The low field MRI image of the cartilage can be clearly defined. The cartilage demonstrated significant greyscale stratification with high greyscale in high water content and low greyscale in low water content. The detail information on the greyscale with respect to the water content of the cartilage was obtain from the low field MRI image. Based on the results, there was significant effect of water content towards the greyscale of the MRI image. These could also denote the potential application of low-field MRI to evaluate the water content of the articular cartilage.

The experimental data obtained from creep indentation test was then incorporated with the simulation of axisymmetric poroelastic finite element model to characterise the permeability and elastic modulus of the cartilage. Based on biphasic theory, cartilage made up from two phases where the solid phase is elastic modulus and fluid phase is permeability. From the results obtained, the water content plays significant role in biomechanical properties and it more significant to elastic modulus. It is important to study the biomechanical properties of the cartilage because the OA can be examine based on this.

© Universiti Teknikal Malaysia Melaka

The main finding of this study was the correlation between the MRI image greyscale and the biomechanical properties of cartilage. There was moderate correlation between MRI image and biomechanical properties. Therefore, further studies on this are required to enhance the study.

5.2 Recommendation

The outcome of this study concluded several findings that would be beneficial to cartilage studies in future research. Besides that, there are few recommendations may be considered that may provide further hypothesis on the greyscale and biomechanical properties of cartilage as well as the correlation between both properties.

In this study, there are some limitations in term of small group size. It is necessary to perform the studies in a large group size in order to obtain more accurate results in greyscale and biomechanical properties of the cartilage. In addition, this study focused on the bovine femoral head specimens. In future, other parts of bovine joint could be considered as the test material specimen.

Furthermore, dehydration of cartilage specimens was carried out in present study. In future, hydration of cartilage specimens could be considered as the test method. In this study, correlation between the cartilage greyscale and biomechanical properties was presented. However, different correlation between the cartilage biomechanical function and biomechanical properties should be further studied so that it could allow for a better diagnostic approach.

© Universiti Teknikal Malaysia Melaka

REFERENCES

Amadò, Renato, Giancarlo Werner, and Hans Neukom. 1976. Water Content of Human Articular Cartilage and Its Determination by Gas Chromatography. Biochemical Medicine 16(2), pp. 169–72.

Armstrong, C. G. 2013. Biphasic Creep and Stress Relaxation of Articular Cartilage in Compression : Theory and Experiments. 102(February 1980), pp. 73–84.

Armstrong, C. G. and V. C. Mow. 1982. Variations in the Intrinsic Mechanical Properties of Human Articular Cartilage with Age, Degeneration, and Water Content. Journal of Bone and Joint Surgery - Series A 64(1), pp. 88–94.

Berberat, Jatta E., Mikko J. Nissi, Jukka S. Jurvelin, and Miika T. Nieminen. 2009. Assessment of Interstitial Water Content of Articular Cartilage with T1 relaxation. Magnetic Resonance Imaging 27(5), pp. 727–32.

Blumenkrantz, Gabrielle and Sharmila Majumdar. 2007. Issn Quantitative Magnetic Resonance Imaging of Articular Cartilage in Osteoarthritis.

Buckwalter, JA ; Mankin,HJ; Grodzinsky, AJ. 2005. 26_BuckwalterArticularCartilage.Pdf. Articular Cartilage and Osteoarthritis 54,pp. 466–80.

Calvo, E., I. Palacios, E. Delgado, J. Ruiz-Cabello, P. Hernández, O. Sánchez-Pernaute, J. Egido, and G. Herrero-Beaumont. 2001. High-Resolution MRI Detects Cartilage Swelling at the Early Stages of Experimental Osteoarthritis. Osteoarthritis and Cartilage 9(5), pp. 463–72.

Carballo, Camila B., Yusuke Nakagawa, Ichiro Sekiya, and Scott A. Rodeo. 2017. Basic Science of Articular Cartilage. Clinics in Sports Medicine 36(3), pp. 413–25.

Chen, A. C., W. C. Bae, R. M. Schinagl, and R. L. Sah. 2001. Depth- and Strain-Dependent Mechanical and Electromechanical Properties of Full-Thickness Bovine Articular Cartilage in Con " Ned Compression. 34.

Currie, Stuart, Nigel Hoggard, Ian J. Craven, Marios Hadjivassiliou, and Iain D. Wilkinson. 2013. Understanding MRI: Basic MR Physics for Physicians. Postgraduate Medical Journal 89(1050), pp. 209–23.

Deyle, Gail D., Nancy E. Henderson, Robert L. Matekel, Michael G. Ryder, Matthew B. Garber, and Stephen C. Allison. 2000. Annals of Internal Medicine, Philadelphia. JAMA: The Journal of the American Medical Association 198(11), pp. 223–27.

Eckstein, F., G. Ateshian, R. Burgkart, D. Burstein, F. Cicuttini, B. Dardzinski, M. Gray, T. M. Link, S. Majumdar, T. Mosher, C. Peterfy, S. Totterman, J. Waterton, C. S. Winalski, and D. Felson. 2006. Proposal for a Nomenclature for Magnetic Resonance Imaging Based Measures of Articular Cartilage in Osteoarthritis. Osteoarthritis and Cartilage 14(10), pp. 974–83.

© Universiti Teknikal Malaysia Melaka

Eckstein, F., F. Cicuttini, J. P. Raynauld, J. C. Waterton, and C. Peterfy. 2006. Magnetic Resonance Imaging (MRI) of Articular Cartilage in Knee Osteoarthritis (OA): Morphological Assessment. Osteoarthritis and Cartilage 14(SUPPL. 1) , pp.46–75.

Egloff, Christian, Thomas Hügle, and Victor Valderrabano. 2012. Biomechanics and Pathomechanisms of Osteoarthritis. (July), pp. 1–14.

Eyre, David. 2002. Collagen of Articular Cartilage. Arthritis Research 4(1), pp. 30–35.

Felson, David T. and Nutrition Examination Survey. 1996. Osteoarthritis and, If. Annals of Internal Medicine. 668–70.

Felson, David T., Yuqing Zhang, John M. Anthony, Allan Naimark, and Jennifer J. Anderson. 2016. Weight Loss Reduces the Risk for Symptomatic Knee Osteoarthritis in Women The Framingham Study. 535–39.

Fox, Alice J. S., Florian Wanivenhaus, and Scott A. Rodeo. 2012. The Basic Science of the Patella: Structure, Composition, and Function. The Journal of Knee Surgery 25(2), pp. 127–41.

Ginat, Daniel T., Michael W. Fong, David J. Tuttle, Susan K. Hobbs, and Rajashree C. Vyas. 2011. Cardiac Imaging: Part 1, MR Pulse Sequences, Imaging Planes, and Basic Anatomy. American Journal of Roentgenology 197(4), pp. 808–15.

Griffin, Michelle, Yaami Premakumar, Alexander Seifalian, Peter Edward Butler, and Matthew Szarko. 2016. Biomechanical Characterization of Human Soft Tissues Using Indentation and Tensile Testing. (December), pp. 1–8.

Gudbergsen, H., M. Boesen, L. S. Lohmander, R. Christensen, M. Henriksen, E. M. Bartels, P. Christensen, L. Rindel, J. Aaboe, B. Danneskiold-Samsøe, B. F. Riecke, and H. Bliddal. 2012. Weight Loss Is Effective for Symptomatic Relief in Obese Subjects with Knee Osteoarthritis Independently of Joint Damage Severity Assessed by High-Field MRI and Radiography. Osteoarthritis and Cartilage 20(6), pp. 495–502.

Hame, Sharon L. and Reginald A. Alexander. 2013. Knee Osteoarthritis in Women. Current Reviews in Musculoskeletal Medicine 6(2), pp. 182–87.

Hannafin, Jo A. and Steven P. Arnoczky. 1994. Effect of Cyclic and Static Tensile Loading on Water Content and Solute Diffusion in Canine Flexor Tendons : An In Vitro Study. 350–56.

Hansen, Pamela, Michael English, and Stuart E. Willick. 2012. Does Running Cause Osteoarthritis in the Hip or Knee? PM and R 4(5 SUPPL.), pp. S117–21.

Hardya, Peter A., Richard Newmark, Yong Mei Liu, Dominik Meier, Steffanie Norris, David W. Piraino, and Amrik Shah. 2000. The Influence of the Resolution and Contrast on Measuring the Articular Cartilage Volume in Magnetic Resonance Images. Magnetic Resonance Imaging 18(8), pp. 965–72.

© Universiti Teknikal Malaysia Melaka

Hayes, W. C. and L. F. Mockros. 1972. A Mathematical Analysis Tests of Articular. 5(December 1970), pp. 541–51.

Hayter, Catherine and Hollis Potter. 2011. Magnetic Resonance Imaging of Cartilage Repair Techniques. The Journal of Knee Surgery 24(4), pp. 225–40.

Huber, Monika, Siegfried Trattnig, and Felix Lintner. 2000. Anatomy, Biochemistry, and Physiology of Articular Cartilage. Investigative Radiology 35(10), pp. 573–80.

Kladny, B., K. Glückert, B. Swoboda, W. Beyer, and G. Weseloh. 1995. Comparison of Low-Field (0.2 Tesla) and High-Field (1.5 Tesla) Magnetic Resonance Imaging of the Knee Joint. Archives of Orthopaedic and Trauma Surgery 114(5), pp. 281–86.

Knecht, Sven, Benedicte Vanwanseele, and Edgar Stüssi. 2006. A Review on the Mechanical Quality of Articular Cartilage - Implications for the Diagnosis of Osteoarthritis. Clinical Biomechanics 21(10), pp. 999–1012.

Kulkarni, Kunal, Timothy Karssiens, Vijay Kumar, and Hemant Pandit. 2016. Obesity and Osteoarthritis. Maturitas 89, pp. 22–28.

Kumar, Rajesh, David M. Pierce, Vidar Isaksen, Catharina De Lange Davies, Jon O. Drogset, and Magnus B. Lilledahl. 2018. Comparison of Compressive Stress-Relaxation Behavior in Osteoarthritic (ICRS Graded) Human Articular Cartilage. International Journal of Molecular Sciences 19(2).

Lee, Christopher S., Shane M. Davis, Claire McGroder, William B. Stetson, and Scott E. Powell. 2013. Analysis of Low-Field Magnetic Resonance Imaging Scanners for Evaluation of Knee Pathology Based on Arthroscopy. Orthopaedic Journal of Sports Medicine 1(7), pp. 1–7.

Lees, Deborah and Paul Partington. 2016. Articular Cartilage. Orthopaedics and Trauma 30(3), pp. 265–72.

Lementowski, Peter W. 2014. Obesity and Osteoarthritis. (April 2008).

Li, X.J, Jonathan Cheng, Katrina Lin, Ehsan Saadat, Radu I. Bolbos, Björn Jobke, Michael D. Ries, Andrew Horvai, Thomas M. Link, and Sharmila Majumdar. 2011. Quantitative MRI Using T1ρand T2in Human Osteoarthritic Cartilage Specimens: Correlation with Biochemical Measurements and Histology. Magnetic Resonance Imaging 29(3), pp. 324–34.

Liess, C., S. Lüsse, N. Karger, M. Heller, and C. G. Glüer. 2002. Detection of Changes in Cartilage Water Content Using MRI T2-Mapping in Vivo. Osteoarthritis and Cartilage 10(12), pp. 907–13.

Link, Richard E. 2006. Analysis of Dynamic Fracture and Crack Arrest of an HSLA Steel in an SE(T) Specimen. Journal of ASTM International 3(1), pp. 63–88.

© Universiti Teknikal Malaysia Melaka

Lories, Rik J. U., Jenny Peeters, Astrid Bakker, Przemko Tylzanowski, Inge Derese, Jan Schrooten, J. Terrig Thomas, and Frank P. Luvten. 2007. Articular Cartilage and Biomechanical Properties of the Long Bones in Frzb-Knockout Mice. Arthritis and Rheumatism 56(12), pp. 4095–4103.

Lu, X., and Mow. 2008. Biomechanics of Articular Cartilage and Determination of Material Properties. (18), pp. 193–99.

Luke, Anthony C., Christoph Stehling, Robert Stahl, Xiaojuan Li, Terry Kay, Stephen Takamoto, Benjamin Ma, Sharmilla Majumdar, and Thomas Link. 2010. High-Field Magnetic Resonance Imaging Assessment of Articular Cartilage before and after Marathon Running: Does Long-Distance Running Lead to Cartilage Damage? American Journal of Sports Medicine 38(11), pp. 2273–80.

Macdonald, Graeme A. and Anthony J. Peduto. 2000. Magnetic Resonance Imaging and Diseases of the Liver and Biliary Tract. Part 2. Magnetic Resonance Cholangiography and Angiography and Conclusions. Journal of Gastroenterology and Hepatology (Australia) 15(9), pp. 992–99.

Mansour, B. Y. Joseph M. 1976. The Permeability of Articular Cartilage under Compressive Strain and at High Pressures *. 58(4), pp. 509–16.

Maroudas, A. 1977. Chemical Composition and Swelling of Normal and Osteoarthrotic Femoral Head Cartilage. 121–29.

Mow, V. C. and W. M. Lai. 1980. Recent Developments in Synovial Joint Biomechanics. Society for Industrial and Applied Mathematics 22(3), pp. 275–317.

Mow, Van C., Mark H. Holmes, and W. Michael Lai. 1984. Fluid Transport and Mechanical Properties of Articular Cartilage: A Review. Journal of Biomechanics 17(5), pp. 377–94.

Ms, Roza Mahmoodian and Jeremi Leasure Bs. 2009. Mechanical Properties of Human Fetal Talus. 1186–94.

Nieminen, M. T. 2004. Proteoglycan and Collagen Sensitive MRI Evaluation of Normal and Degenerated Articular Cartilage. 22:557–64.

Nieminen, Miika T., Juha Töyräs, Mikko S. Laasanen, Johanna Silvennoinen, Heikki J. Helminen, and Jukka S. Jurvelin. 2004. Prediction of Biomechanical Properties of Articular Cartilage with Quantitative Magnetic Resonance Imaging. Journal of Biomechanics 37(3), pp. 321–28.

Niinima, M., R. Lindgren, M. T. Nieminen, I. Kiviranta, and J. S. Jurvelin. 2001. Estimation of the Young's Modulus of Articular Cartilage Using an Arthroscopic Indentation Instrument and Ultrasonic Measurement of Tissue Thickness. 34, pp. 251–56.

© Universiti Teknikal Malaysia Melaka

Park, C. T. Hung Ph D, and G. A. Ateshian Ph D. 2004. Mechanical Response of Bovine Articular Cartilage under Dynamic Unconfined Compression Loading at Physiological Stress Levels. 65–73.

Pawaskar, Sainath Shrikant, John Fisher, and Zhongmin Jin. 2010. Robust and General Method for Determining Surface Fluid Flow Boundary Conditions in Articular Cartilage Contact Mechanics Modeling. Journal of Biomechanical Engineering 132(3), pp. 031001.

Pereira, D., B. Peleteiro, J. Araújo, J. Branco, R. A. Santos, and E. Ramos. 2011. The Effect of Osteoarthritis de Fi Nition on Prevalence and Incidence Estimates : A Systematic Review. Osteoarthritis and Cartilage 19(11), pp. 1270–85.

Peterfy, Charles G., A. Guermazi, S. Zaim, P. F. J. Tirman, Y. Miaux, D. White, M. Kothari, Y. Lu, K. Fye, S. Zhao, and H. K. Genant. 2004. Whole-Organ Magnetic Resonance Imaging Score (WORMS) of the Knee in Osteoarthritis. Osteoarthritis and Cartilage 12(3), pp. 177–90.

Peters, Abby E., Riaz Akhtar, Eithne J. Comerford, and Karl T. Bates. 2018. The Effect of Ageing and Osteoarthritis on the Mechanical Properties of Cartilage and Bone in the Human Knee Joint. Scientific Reports (June 2017), pp. 1–13.

Ph, D., L. M. S. Pillet, A. M. S. Inaebnit, and O. M. D. Borens. 2006. Biomechanical Characterization and in Vitro Mechanical Injury of Elderly Human Femoral Head Cartilage : Comparison to Adult Bovine Humeral Head Cartilage.

Przeworski, A., Z. Adamiak, and J. Głodek. 2016. Comparison of High-Field and Low-Field Magnetic Resonance Imaging of Stifle Joint Disorders in Dogs. Polish Journal of Veterinary Sciences 19(3), pp. 663–70.

Raleigh, A. R., W. J. McCarty, A. C. Chen, C. Meinert, T. J. Klein, and R. L. Sah. 2017. Synovial Joints: Mechanobiology and Tissue Engineering of Articular Cartilage and Synovial Fluid. Reference Module in Materials Science and Materials Engineering 6, pp. 199–212.

Raynauld, Jean Pierre, Johanne Martel-Pelletier, Marie Josée Berthiaume, Françoys Labonté, Gilles Beaudoin, Jacques A. De Guise, Daniel A. Bloch, Denis Choquette, Boulos Haraoui, Roy D. Altman, Marc C. Hochberg, Joan M. Meyer, Gary A. Cline, and Jean Pierre Pelletier. 2004. Quantitative Magnetic Resonance Imaging Evaluation of Knee Osteoarthritis Progression over Two Years and Correlation with Clinical Symptoms and Radiologic Changes. Arthritis and Rheumatism 50(2), pp. 476–87.

Rodrigues, Marcelo Bordalo and Gilberto Luís Camanho. 2010. Mri Evaluation of Knee Cartilage. Revista Brasileira de Ortopedia (English Edition) 45(4), pp. 340–46.

Roemer, F. W., J. A. Lynch, J. Niu, Y. Zhang, M. D. Crema, I. Tolstykh, G. Y. El-Khoury, D. T. Felson, C. E. Lewis, M. C. Nevitt, and A. Guermazi. 2010. A Comparison of Dedicated 1.0 T Extremity MRI vs Large-Bore 1.5 T MRI for Semiquantitative Whole

© Universiti Teknikal Malaysia Melaka

Organ Assessment of Osteoarthritis: The MOST Study. Osteoarthritis and Cartilage 18(2), pp. 168–74.

Rutt, Brian K. and Donald H. Lee. 1996. The Impact of Field Strength on Image Quality in MRI. Journal of Magnetic Resonance Imaging 6(1), pp. 57–62.

Shapiro, Lauren M., Emily J. McWalter, Min Sun Son, Marc Levenston, Brian A. Hargreaves, and Garry E. Gold. 2014. Mechanisms of Osteoarthritis in the Knee: MR Imaging Appearance. Journal of Magnetic Resonance Imaging 39(6), pp. 1346–56.

Shiguetomi-Medina, J. M., J. L. Ramirez-GL, H. Stødkilde-Jørgensen, and B. Møller-Madsen. 2017. Systematized Water Content Calculation in Cartilage Using T1-Mapping MR Estimations: Design and Validation of a Mathematical Model. Journal of Orthopaedics and Traumatology 18(3), pp. 217–20.

Sotres, Javier and Thomas Arnebrant. 2013. Experimental Investigations of Biological Lubrication at the Nanoscale: The Cases of Synovial Joints and the Oral Cavity. 102–31.

Srikanth, Velandai K., Jayne L. Fryer, Guangju Zhai, Tania M. Winzenberg, David Hosmer, and Graeme Jones. 2005. A Meta-Analysis of Sex Differences Prevalence, Incidence and Severity of Osteoarthritis. Osteoarthritis and Cartilage 13(9), pp. 769–81.

Taouli, Bachir, Souhil Zaim, Charles G. Peterfy, John A. Lynch, Alexander Stork, Ali Guermazi, Bo Fan, Kenneth H. Fye, and Harry K. Genant. 2004. Rheumatoid Arthritis of the Hand and Wrist: Comparison of Three Imaging Techniques. American Journal of Roentgenology 182(4), pp. 937–43.

Taruc-Uy, Rafaelani L. and Scott A. Lynch. 2013. Diagnosis and Treatment of Osteoarthritis. Primary Care - Clinics in Office Practice 40(4), pp. 821–36.

Uth, Kristin and Dimitar Trifonov. 2014. Stem Cell Application for Osteoarthritis in the Knee Joint : A Minireview. 6(5), pp. 629–36.

Yew W.S., Mohd Juzaila Abd Latif, and Norhashimah Mohd Saad. 2017. Characterization of Articular Cartilage Using Low-Field Magnetic Resonance Imaging Image. 7(6), pp. 1149–52.

Wirtz, C. R. and N. Aras. 2001. Low-Field Interventional MRI in Neurosurgery : Finding the Right Dose of Contrast Medium. 254–58.

Woertler, Klaus, Marc Strothmann, Bernd Tombach, and Peter Reimer. 2000. Detection of Articular Cartilage Lesions: Experimental Evaluation of Low- and High-Field-Strength MR Imaging at 0.18 and 1.0 T. Journal of Magnetic Resonance Imaging 11(6), pp. 678–85.

Xu, Jiadi, Peizhi Zhu, Michael D. Morris, and Ayyalusamy Ramamoorthy. 2011. Solid-State NMR Spectroscopy Provides Atomic-Level Insights Into the Dehydration of Cartilage. 9948–54.

© Universiti Teknikal Malaysia Melaka

Yang, C-j, J-f Zhang, Y. Chen, Y-m Dong, and Y. Zhang. 2008. Proceedings of the Institution of Mechanical Engineers, Part C : Journal of Mechanical Engineering Science A Review of Exoskeleton-Type Systems and Their Key Technologies.

Zamli, Zaitunnatakhin and Mohammed Sharif. 2011. Chondrocyte Apoptosis : A Cause or Consequence of Osteoarthritis ? 159–66.

UNIVERSITI TEKNIKAL MALAYSIA MELAKA

© Universiti Teknikal Malaysia Melaka

APPENDIX A

Matlab script

```
x=dicomread('F:\DICOM\Filename');
info=dicominfo('F:\DICOM\Filename');
y=dicomread(info);
figure,imshow(y);
imcontrast;
X2=imcrop(x,maps,[xmin ymin 32 32]);
subplot (1,2,1);
imshow(x, maps);
title ('Original Image');
subplot (1,2,2);
imshow(X2,maps);
title ('Cropped Image');
whos;
```

UNIVERSITI TEKNIKAL MALAYSIA MELAKA

© Universiti Teknikal Malaysia Melaka

APPENDIX B

Water Content of Cartilage Specimen

	S1	S2	S3	S4	S5	S6
Initial	0.73935	0.75495	0.72248	0.83616	0.78754	0.76810
30 min	0.67012	0.73042	0.66903	0.80738	0.76914	0.72921
60 min	0.59780	0.67922	0.52745	0.76304	0.73876	0.66125
90 min	0.44333	0.58948	0.45817	0.71360	0.69195	0.57931
120 min	0.36148	0.44372	0.36770	0.58396	0.62984	0.47734

UNIVERSITI TEKNIKAL MALAYSIA MELAKA

© Universiti Teknikal Malaysia Melaka

APPENDIX C

Thickness of Cartilage Specimen

Specimen	Thickness, mm
1	0.867
2	1.535
3	1.338
4	1.272
5	1.438
6	1.554
7	1.077

UNIVERSITI TEKNIKAL MALAYSIA MELAKA

© Universiti Teknikal Malaysia Melaka